

# Theory and Modeling of the Zeeman and Paschen-Back effects in Molecular Lines

A. Asensio Ramos, J. Trujillo Bueno<sup>1</sup>

*Instituto de Astrofísica de Canarias, 38200, La Laguna, Spain*

aasensio@iac.es, jtb@iac.es

## ABSTRACT

This paper describes a very general approach to the calculation of the Zeeman splitting effect produced by an external magnetic field on the rotational levels of diatomic molecules. The method is valid for arbitrary values of the total electronic spin and of the magnetic field strength -that is, it holds for molecular electronic states of any multiplicity and for both the Zeeman and incomplete Paschen-Back regimes. It is based on an efficient numerical diagonalization of the effective Zeeman Hamiltonian, which can incorporate easily all the contributions one may eventually be interested in, such as the hyperfine interaction of the external magnetic field with the spin motions of the nuclei. The reliability of the method is demonstrated by comparing our results with previous ones obtained via formulae valid only for doublet states. We also present results for molecular transitions arising between non-doublet electronic states, illustrating that their Zeeman patterns show signatures produced by the Paschen-Back effect.

*Subject headings:* magnetic fields — polarization — molecular processes — methods: numerical

## 1. Introduction

Most polarized radiation diagnostics of astrophysical magnetic fields have been carried out via the theoretical interpretation of the observed polarization signatures in *atomic* spectral lines (e.g., the reviews by Bagnulo 2003; Mathys 2002; Stenflo 2002). However, over the last few years we have witnessed an increasing interest in molecular spectropolarimetry as a tool for empirical investigations on solar and stellar magnetism, concerning both the molecular Zeeman effect (e.g., the recent overviews by Asensio Ramos & Trujillo Bueno 2003; Berdyugina et al. 2003 and Landi Degl’Innocenti 2003a; see also Uitenbroek et al. 2004) and the Hanle effect in molecular lines (e.g., Landi Degl’Innocenti 2003b; Trujillo Bueno 2003a).

---

<sup>1</sup>Consejo Superior de Investigaciones Científicas, Spain

The aim of the present paper is to describe in some detail our approach to the Zeeman and Paschen-Back effects in diatomic molecular lines, which we have been applying over the last few years while contributing to the development of the field of radiative transfer in molecular lines (Asensio Ramos & Trujillo Bueno 2003, 2005; Asensio Ramos et al. 2003, 2004a, 2004b, 2005). Our strategy is based on a very efficient numerical diagonalization of the effective Zeeman Hamiltonian, whose general expression has been derived by a number of authors working in the field of molecular physics (e.g., Brown & Carrington 2003). Interestingly, in physics laboratory experiments, where the applied magnetic field is known beforehand, the observation of the splittings provide a measurement of the magnetic dipole moment of the considered molecule in the particular spin-rotational level involved. Given that the magnetic moment depends on the electronic structure of the molecule, it is obvious that its measurement provides information about the molecular structure. In astrophysics we have the inverse problem, the magnetic field being the unknown quantity. To obtain information about cosmic magnetic fields, therefore, we have to make use of our most precise knowledge on molecular structure in order to infer the magnetic field vector via the theoretical modeling of polarization signals in molecular lines. To this end, we need:

- to obtain the molecular number densities at each point within the astrophysical plasma model under consideration,
- to calculate the splittings of the molecular energy levels with the strengths of the individual Zeeman components, and
- to solve the radiative transfer problem for the emergent Stokes parameters.

Here we focus on the issue of calculating the splittings and strengths of molecular transitions, including the most general situation of the incomplete Paschen-Back effect for electronic states of arbitrary multiplicity. For information on the techniques we use for calculating the molecular number densities and for solving the Stokes-vector radiative transfer problem in (magnetized) stellar atmospheres we refer the reader to the papers by Asensio Ramos et al. (2003) and Trujillo Bueno (2003b), respectively.

It is of historical interest to mention that the Zeeman effect in diatomic molecules was considered shortly after the development of the quantum theory. Kronig (1928) investigated the molecular Zeeman effect in Hund’s (a) and (b) cases for the angular momentum coupling between electronic and rotational motion. Only one year after, Hill (1929) investigated the Zeeman effect for doublet states of diatomic molecules in intermediate states between Hund’s cases (a) and (b). The status of the theory was reviewed by Crawford (1934), emphasizing that, at that moment, the Zeeman effect was understood in pure Hund’s cases (a) and (b) and in intermediate cases between the two. At that time, the intensity of the Zeeman transitions had not been investigated in detail because the calculations were rather involved when using the basis functions of Hund’s case (b). Fifty years after the paper of Kronig, Schadee (1978) re-investigated the Zeeman effect for doublet states of diatomic lines in the intermediate case between Hund’s cases (a) and (b), but using the basis

functions of Hund’s case (a). This greatly facilitated the calculation of the intensity of the Zeeman transitions. The issue of the Zeeman effect in lines of diatomic molecules was later considered by Illing (1981) who studied in great detail Schadee’s (1978) theory and applied it for understanding the broad-band *circular* polarization observed by Harvey (1973) in near-IR lines of CN.

All the above-mentioned developments were based on a number of approximations for the description of the molecular motions for the zero field case. They take into account the rotational energy (but neglecting centrifugal distortions) and the strongest angular momenta couplings. For states without electronic orbital angular momentum ( $\Sigma$  states), only the spin-rotation coupling was included. For states with non-zero electronic orbital angular momentum ( $\Pi$ ,  $\Delta$ , ...), only the spin-orbit coupling was taken into account.

The formulae developed by Schadee (1978) are only applicable to doublet states of diatomic molecules in the Zeeman or Paschen-Back regimes. Recently, Berdyugina & Solanki (2002) have extended Schadee’s (1978) formulation to allow for the calculation of the effect of a magnetic field on states with arbitrary spin, but limited to the Zeeman regime. Their strategy consisted in numerically diagonalizing a simplified Hamiltonian corresponding to the zero-field case and accounting for the Zeeman Hamiltonian as a first order perturbation. This approach, which neglects the non-diagonal matrix elements ( $\Delta J \neq 0$ ) of the Zeeman Hamiltonian, is only valid in the linear Zeeman regime. Therefore, the maximum reliable value of the magnetic field strength is established by the transition to the Paschen-Back regime.

In this paper we present a very general approach which allows us to calculate the effect of a magnetic field on the rotational levels of diatomic molecules in electronic states with arbitrary multiplicity. The method is valid in both the Zeeman and the Paschen-Back regimes. It is based on the numerical diagonalization of the effective molecular Hamiltonian, which describes the molecular motion using the basis functions of Hund’s case (a). Therefore, the inclusion of any additional contribution to the effective Hamiltonian of the diatomic molecule is straightforward, provided the matrix elements of the Hamiltonian are known in the basis functions of Hund’s case (a). This makes it possible to investigate effects like hyperfine structure (HFS) without much additional effort. Such refinements are not only of interest in physics laboratory experiments, but also when it comes to interpreting correctly the linear polarization signals that anisotropic radiation pumping processes induce in spectral lines (e.g., Landi Degl’Innocenti & Landolfi 2004). The illustrative examples shown in this paper neglect HFS effects, but we plan to consider this interesting molecular HFS problem in a future investigation.

The outline of this paper is the following. Section 2 and the various appendices describe our numerical diagonalization approach in some detail, including a summary of some results from angular momentum theory with the aim of facilitating a better understanding of the paper. In order to verify the reliability of our numerical results, in Section 3 we compare them with those that can be obtained via Schadee’s (1978) theory. We will show also some applications to non-doublet states. Finally, Section 4 summarizes our main conclusions with an outlook to future research.

## 2. Angular momentum theory for diatomic molecules

The theory of angular momentum provides a robust theoretical framework for describing the complex structure of diatomic molecules. In this section we summarize how the angular momentum theory and Racah’s tensor algebra allow the description of the quantum mechanical behavior of any diatomic molecule under the presence of an arbitrary magnetic field. Although the theory on which our work is based on can be found explained in detail in specialized monographs on molecular spectroscopy (e.g., Judd 1975, Brown & Carrington 2003), we have decided to present here a brief summary in order to facilitate the understanding of this paper and to avoid any possible notational confusion.

### 2.1. Introduction

As is well-known, the Born-Oppenheimer approximation leads to an effective separation of the energies due to the electronic, vibrational and rotational motions in molecules (e.g., Herzberg 1950). This approximation is supported by the fact that the mass of the nuclei is several orders of magnitude larger than the mass of the electrons. This implies that, when nuclei move, the electrons adapt rapidly to the new nuclear configuration. As a result, the electrons feel some kind of effective potential, which depends only on the positions of the nuclei and on the electronic configuration of the particular electronic state. The Born-Oppenheimer approximation immediately leads to the possibility of separating the eigenfunctions associated with each motion.

For convenience, we have selected Hund’s case (a) eigenfunctions because they lead to several simplified expressions (see Appendix A for details). In particular, the eigenvalues of the angular momentum operators are very easy to obtain in this basis set, which greatly simplifies the calculation of the matrix elements of the total Hamiltonian. The obvious consequence of selecting a basis set, which is a truly good basis only in some limiting conditions, is that the total Hamiltonian is usually non-diagonal and it has to be diagonalized to obtain the energies of the molecular levels. In the usual notation, the Hund’s case (a) eigenfunctions can be written as (Judd 1975):

$$|\alpha\Lambda S\Sigma; v; \Omega JM\rangle \equiv |\alpha\Lambda S\Sigma\rangle|v\rangle|\Omega JM\rangle, \quad (1)$$

where we have explicitly indicated that the total eigenfunction is a product of the eigenfunctions associated with the electronic, vibrational and rotational motions (which is only strictly valid under the Born-Oppenheimer approximation).

We point out that  $|\alpha\Lambda S\Sigma\rangle$  is the electronic eigenfunction. The symbol  $\alpha$  represents a collection of quantum numbers which are used to label the electronic configuration of the molecule, while  $S$  is the total spin. The symbols  $\Lambda$  and  $\Sigma$  are the projections of the total orbital electronic angular momentum ( $\mathbf{L}$ ) and of the total spin ( $\mathbf{S}$ ) on the internuclear axis, respectively. Both are good quantum numbers in Hund’s case (a), while  $\Sigma$  is not a good quantum number in Hund’s case (b) (see Appendix A for more details). The vibrational eigenfunction is represented by  $|v\rangle$ . Because

we are interested in lines of diatomic molecules, this eigenfunction can be correctly described with only one quantum number  $v$ . Finally,  $|\Omega JM\rangle$  represents the rotational eigenfunction. This function depends on the total angular momentum  $J$ , its projection  $M$  on the quantization axis (typically chosen as the axis along the magnetic field vector) and the number  $\Omega = |\Lambda| + \Sigma$ . It is interesting to note that  $\Omega$  is a good quantum number only in Hund’s (a) case, since  $\Sigma$  is only well defined in this case. Note also that, due to the presence of the absolute value, in the non-rotating molecule the energy of the spin-orbit levels with  $\Omega \geq 1/2$  are doubly degenerate. When the molecule is rotating, this degeneracy is broken (see, e.g. Herzberg 1950). A brief summary of the good quantum numbers in Hund’s cases (a) and (b) can be found in Table 1. Additionally, vector diagrams of the two coupling cases are shown in Figure 11, which clearly show the strength of each coupling.

Due to the difference in mass between the electrons and the nuclei of the diatomic molecule, it is appropriate to refer the motion of the electrons to a frame  $F'$  fixed to the nuclei whose origin is at the center of mass of the molecule, rather than to an external laboratory frame  $F$  (with its origin also at the center of mass of the molecule). Fig. 1 illustrates the relative position of both frames. The coordinates of an electron in the laboratory frame  $F$  are  $(x, y, z)$ , while the coordinates on the frame fixed to the molecule  $F'$  are  $(\xi, \eta, \zeta)$ . Given the arbitrariness in the choice of the frames, it is convenient to consider the  $\zeta$  axis of the  $F'$  frame parallel to the internuclear axis and the  $z$  axis of the  $F$  frame along the quantization axis. This quantization axis is usually chosen along the direction of the magnetic field vector when it is present. Obviously, in the absence of a magnetic field, it can be arbitrarily chosen in any direction. Since both reference frames share the same origin, coordinates in one frame can be transformed to the other frame by means of a simple rotation. This rotation can be parameterized in terms of the three Euler angles  $(\alpha, \beta, \gamma)$ . Once the coordinates of an electron are known in one of the frames, a standard geometrical rotation between both frames using the Euler angles can be used to obtain the coordinates in the other frame. As usual, once the  $\zeta$  axis of the  $F'$  frame is fixed, there is an additional freedom in the choice of the direction of the  $\xi$  and  $\eta$  axis, which depends on our choice for the Euler angle  $\gamma$ . Without loss of generality, we choose  $\gamma = \pi/2$ .

The normalized rotational eigenfunctions  $|\Omega JM\rangle$  in Hund’s case (a) can be obtained by solving the Schrödinger equation for a symmetric top. The solution depends explicitly on the Euler angles, and can be written as (Judd 1975)

$$|\Omega JM\rangle = \sqrt{\frac{2J+1}{8\pi^2}} \mathcal{D}_{M\Omega}^J(\alpha, \beta, \gamma)^*, \quad (2)$$

where  $\mathcal{D}_{M\Omega}^J(\alpha, \beta, \gamma)$  is the rotation matrix (e.g., Edmonds 1960). The representation of the rotational eigenfunctions in terms of the rotation matrices is very convenient because it facilitates the subsequent calculations. A fundamental property is that of conjugation for the rotation matrices, which can be expressed as

$$\mathcal{D}_{M\Omega}^J(\alpha, \beta, \gamma)^* = (-1)^{M-\Omega} \mathcal{D}_{-M-\Omega}^J(\alpha, \beta, \gamma). \quad (3)$$

Other important properties of the rotation matrices which are used in this section are summarized

in Appendix B. Note that the conjugation property allows us to verify that the rotational eigenfunctions are orthonormal. In fact, one can apply Eq. (3) together with Eq. (B2) to verify that  $\langle \Omega' J' M' | \Omega J M \rangle = \delta_{\Omega' \Omega} \delta_{J' J} \delta_{M' M}$ .

The rotation matrices are of great help for transforming tensorial operators from one frame to another, provided that the Euler angles between both frames are known. Given that we are dealing with rotations, it is advantageous to consider the spherical components of a tensor instead of working with the cartesian ones (see, e.g., Edmonds 1960 for the definition of the spherical components of a tensor). Let us consider in some detail the case of a vector, since it will be helpful for calculating the matrix elements of the Hamiltonian. Assume that  $\mathbf{r}$  is a vector in  $\mathbb{R}^3$  whose spherical components in the laboratory frame  $F$  are given by  $\bar{r}_q$ , where  $q = 0, \pm 1$ . The spherical components of the same vector in the frame fixed to the molecule  $F'$  are denoted by  $r_q$ . The relationship between both components can be written as (e.g., Edmonds 1960):

$$\bar{r}_q = \sum_{q'=0,\pm 1} r_q \mathcal{D}_{q'q}^1(-\alpha, -\beta, -\gamma), \quad (4)$$

where we have used the fact that the rotation needed to carry the frame fixed to the molecule to the laboratory frame is expressed by the inverse rotation  $(-\alpha, -\beta, -\gamma)$ . Using the properties of the rotation matrices (see, e.g., Edmonds 1960), the previous equation can also be written as:

$$\bar{r}_q = \sum_{q'=0,\pm 1} r_q \mathcal{D}_{qq'}^1(\alpha, \beta, \gamma)^*. \quad (5)$$

The final part of this introduction to the mathematical tools needed to calculate the matrix elements of the Hamiltonian is related to the Wigner-Eckart (WE) theorem (e.g., Edmonds 1960). This theorem facilitates the calculation of the matrix element of any tensor operator because it takes full advantage of any symmetry that may be inherent to the problem under consideration. In other words, it isolates those parts of a problem that are essentially geometric in character from those which depend explicitly on the physics of the problem. For the  $q$  component of a given tensor of rank  $k$ , the WE theorem reads:

$$\langle JM | T_q^{(k)} | J' M' \rangle = (-1)^{J-M} \begin{pmatrix} J & k & J' \\ -M & q & M' \end{pmatrix} \langle J || T^{(k)} || J' \rangle. \quad (6)$$

The quantity  $\langle J || T^{(k)} || J' \rangle$  is called the reduced matrix element, a number which depends on the physics of the selected problem. An example is the reduced matrix element that involves an angular momentum  $\mathbf{J}$  between its own eigenfunctions:

$$\langle J || \mathbf{J} || J \rangle = \sqrt{J(J+1)(2J+1)} \quad (7)$$

## 2.2. Molecular Hamiltonian

In this section we present the total effective Hamiltonian which we use to describe the molecular motion including the effect of a magnetic field. Consider a diatomic molecule in a given

electronic, vibrational and rotational state and in the presence of an external magnetic field. It is possible to describe the molecular motion by writing the full Hamiltonian which takes into account all the Coulomb forces among electrons and nuclei and the Lorentz force due to the presence of a magnetic field. However, it is more appropriate in terms of both economy and feasibility to consider the effective Hamiltonian approach (Brown et al. 1979, Brown & Carrington 2003). This effective Hamiltonian has the same eigenvalues as the full Hamiltonian, but it operates only within the rotational, spin and hyperfine levels of a given vibrational level belonging to a given electronic state. The non-diagonal matrix elements (coupling the vibrational level of interest with any other vibrational level of any other electronic state) are absorbed in the effective Hamiltonian and represented by some parameters which can be obtained by comparison with laboratory or astrophysical observations. Following Brown & Carrington (2003) (see also Brown et al. 1979) we write down the following very general expression for the *effective Hamiltonian*:

$$\begin{aligned}
 H_{\text{eff}} &= H_{\text{SO}} + H_{\text{SS}} + H_{\text{rot}} + H_{\text{cd}} + H_{\text{sr}} + H_{\text{LD}} \\
 &+ H_{\text{cdLD}} + H_{\text{hfs}} + H_{\text{cdhfs}} + H_Z.
 \end{aligned}
 \tag{8}$$

The term  $H_{\text{SO}}$  represents the coupling between the total spin of the molecule  $\mathbf{S}$  and the orbital angular momentum  $\mathbf{L}$ .  $H_{\text{SS}}$  represents the coupling between the spins of the electrons in the molecule. The rotational energy of the molecule is accounted for by the term  $H_{\text{rot}}$ , while  $H_{\text{cd}}$  represents the contribution to the rotational energy of the centrifugal distortion as a consequence of the rotation of the molecule. The interaction between the total molecular spin and the rotational angular momentum is described by  $H_{\text{sr}}$ . The additional degeneracy present for the two possible projections of  $\mathbf{L}$  on the internuclear axis, namely  $\pm|\Lambda|$ , is broken by the inclusion of the terms  $H_{\text{LD}}$  and  $H_{\text{cdLD}}$  of the effective Hamiltonian. These terms represent the  $\Lambda$ -doubling interactions (interaction with higher energy electronic states) and the appropriate centrifugal distortion corrections, respectively. In case one is interested in taking into account the hyperfine structure, it suffices to include the terms  $H_{\text{hfs}}$  and  $H_{\text{cdhfs}}$ , which are the hyperfine interaction and the corresponding centrifugal distortion of the hyperfine interaction as the molecule rotates, respectively. Such hyperfine contributions will not be considered in this paper, but they will be the subject of a future investigation. Finally,  $H_Z$  represents the interaction between the molecule and an external magnetic field  $\mathbf{B}$ .

Each one of the terms of the Hamiltonian can be written with the aid of the different angular momentum operators that can be defined in the molecule. As previously mentioned, it is useful to write all these operators using the spherical tensor notation because it leads to considerable simplifications in the notation and it allows the use of the powerful tools of the angular momentum theory. The same notation we have used for vectors can be straightforwardly extended to the spherical components of tensorial operators. On the one hand,  $A_q^k$  will refer to the  $q$  spherical component of the tensor  $\mathbf{A}^k$  of rank  $k$  in the molecular fixed frame  $F'$ . On the other hand, the spherical component of the same tensor in the laboratory frame  $F$  will be indicated by  $\bar{A}_q^k$ . This extension to tensors of arbitrary rank  $k$  is only needed when we include in the Hamiltonian tensorial operators (see, e.g., Brown & Carrington 2003). In the effective Hamiltonian used in this paper we consider only vectorial operators with rank up to  $k = 1$ . However, it is important to emphasize

that this formalism allows us to include any contribution to the effective Hamiltonian written in terms of tensorial operators, which constitutes one of its big advantages.

The explicit form of each of the terms included in the effective Hamiltonian has been obtained previously by molecular physicists (see Brown & Carrington 2003, and references therein). The effective Hamiltonian approach is flexible enough to allow writing the explicit form of some of the terms of the Hamiltonian in different ways. It is advantageous to write them in a way that simplifies the calculation of the matrix elements in the chosen basis set. The spin orbit coupling term reads

$$H_{\text{SO}} = AL_0^1 S_0^1 + \frac{1}{2}A_D [\mathbf{N}^2 L_0^1 S_0^1 + L_0^1 S_0^1 \mathbf{N}^2], \quad (9)$$

where  $A$  and  $A_D$  are the spin-orbit coupling constant and the centrifugal correction to  $A$ , respectively. The first part includes the coupling between the total spin and the orbital angular momentum. Note that this contribution using Hund’s case (a) basis set is just proportional to the product of  $\Lambda$  and  $\Sigma$  since these are the  $L_0^1$  and  $S_0^1$  components of  $\mathbf{L}$  and  $\mathbf{S}$ , respectively. The second term includes the effect of the centrifugal distortion in the spin-orbit coupling. The symbol  $\mathbf{N}^2$  stands for the scalar product of  $\mathbf{N}$  by itself, i.e.,  $\mathbf{N}^2 = \mathbf{N} \cdot \mathbf{N}$ . Following Brown & Carrington (2003), we use  $\mathbf{N}^2$  as the square of the rotational operator instead of  $\mathbf{R}^2$  (see Appendix A). The latter approach is preferred by some authors because this operator is proportional to the rotational kinetic energy. However, using  $\mathbf{R}$  as the rotational operator involves the angular momentum  $\mathbf{L}$  which has non-diagonal elements between different electronic levels. In the effective Hamiltonian approach, the effect of these non-diagonal terms are absorbed into the rotational and coupling constants. This way, we end up with a Hamiltonian which operates only within the (rotational, spin and hyperfine) levels of a given vibrational level of an individual electronic state.

Focusing now on the spin-spin interaction, several functional forms have been suggested in the literature (e.g., Brown & Carrington 2003 for a summary). It has been shown that they are equivalent and we have decided to choose the following functional form which greatly simplifies the calculation of the matrix elements in Hund’s case (a) basis set:

$$H_{\text{SS}} = \frac{2}{3}\lambda [3(S_0^1)^2 - \mathbf{S}^2], \quad (10)$$

where  $\lambda$  is the spin-spin coupling constant. Obviously, this contribution turns out to be important only when more than one electron is uncoupled ( $S > 1/2$ ).

Turning our attention to the rotational part of the effective Hamiltonian, the pure rotation Hamiltonian can be written as

$$H_{\text{rot}} = B\mathbf{N}^2, \quad (11)$$

where  $B$  is the usual rotational constant. For the evaluation of the matrix elements in the basis set of Hund’s case (a), it is better to represent the rotational angular momentum  $\mathbf{N}$  in terms of  $\mathbf{J}$  and  $\mathbf{S}$  since these operators have well-defined eigenvalues in this basis set. This transformation can be easily carried out because  $\mathbf{N} = \mathbf{J} - \mathbf{S}$  (see Appendix A). Concerning the inclusion of centrifugal



distortion terms, it is sufficient to arrive up to the third order contribution even for laboratory experiments, and the explicit form of the Hamiltonian turns out to be:

$$H_{\text{cd}} = -D(\mathbf{N}^2)^2 + H(\mathbf{N}^2)^3, \quad (12)$$

where  $D$  and  $H$  are the quartic and sextic distortion constants. Finally, the coupling of the spin and the rotation can be included in the effective Hamiltonian as the scalar product between the rotational angular momentum and the spin:

$$H_{\text{sr}} = \gamma(\mathbf{J} - \mathbf{S}) \cdot \mathbf{S}, \quad (13)$$

where  $\gamma$  is the spin-rotation coupling constant (note that this constant is different from the  $\gamma$  Euler angle). In this paper we will not include more terms in the effective Hamiltonian for the zero-field case.

An additional constraint has to be included when dealing with diatomic molecules that greatly simplifies the evaluation of the matrix elements of the effective Hamiltonian. This constraint is related to the fact that the molecule does not rotate around the internuclear axis and so  $(J_0^1 - L_0^1 - S_0^1) = 0$  (where the 0 component of the rotational angular momentum operator is along the internuclear axis due to the selection of the frame  $F'$ ).

When the molecule is under the action of a magnetic field  $\mathbf{B}$ , the magnetic sublevels pertaining to each energy level of total angular momentum  $J$  have slightly different energies, essentially due to the precession of the total angular momentum around the quantization  $z$ -axis, which we have chosen along the magnetic field vector. It is possible to write a Zeeman effective Hamiltonian for a diatomic molecule that takes into account the coupling between the magnetic field  $\mathbf{B}$  and the total spin  $\mathbf{S}$  and orbital angular momentum  $\mathbf{L}$  and between the magnetic field and the rotation of the molecule  $\mathbf{N} = \mathbf{J} - \mathbf{S}$ :

$$\begin{aligned} H_Z &= g_S \mu_0 \mathbf{B} \cdot \mathbf{S} + g_L \mu_0 \mathbf{B} \cdot \mathbf{L} \\ &- g_r \mu_0 \mathbf{B} \cdot (\mathbf{J} - \mathbf{S}), \end{aligned} \quad (14)$$

where  $\mu_0$  is the Bohr magneton,  $B$  is the magnetic field vector,  $g_S$  is the electron spin  $g$ -factor,  $g_L$  is the electron orbital  $g$ -factor and  $g_r$  is the rotational  $g$ -factor (including the nuclear and electronic contribution  $g_r = g_r^{\text{nuclear}} - g_r^{\text{elec}}$ ). If the spin of the nuclei is non-zero, a contribution of the coupling between the nuclear spins and the magnetic field can be included with:

$$H_Z^{\text{nuc}} = \sum_1 g_N^i \mu_N \mathbf{B} \cdot \mathbf{I}^i, \quad (15)$$

where the nuclei are labeled by  $i$ . Because we neglect hyperfine structure, we will also neglect this term.

Although small differences exist, it is usual to put  $g_S = 2$  and  $g_L = 1$ . The exact value of  $g_S$  is slightly larger than 2 (its value can be obtained from Quantum Electrodynamical considerations)

and in fact the values of the  $g$ -factors can be slightly different due to the inclusion of additional perturbations from other electronic states. On the contrary, due to the difference of mass between the electron and the proton, the rotational  $g$ -factor (which is of the order of  $\mu_N/\mu_0$ , with  $\mu_N$  the nuclear magneton) is  $\sim 3$  orders of magnitude smaller than the electronic  $g$ -factors. Therefore, the contribution of the last term of the Zeeman Hamiltonian is only relevant when the molecule has no spin and no orbital angular momentum. In this case, there is no contribution to the Zeeman effect coming from the electronic motion because the electronic cloud is essentially spherical and the molecule is in a  $^1\Sigma$  state. This is the case of the fundamental electronic states of CO and SiO, for which the sensitivity to the presence of a magnetic field is very small. Ideally, the value of the  $g$ -factors should be determined by confronting the theoretical description of the molecule with spectroscopic observations. The rotational  $g$ -factor includes a pure nuclear contribution and another one coming from the coupling between the rotation of the electronic cloud and the magnetic field (Judd 1975). The nuclear contribution to the rotational  $g$ -factor for a diatomic molecule formed by two nuclei A and B can be estimated by the following formula (Judd 1975):

$$g_r^{\text{nuclear}} \simeq \frac{\mu_N}{\mu_0} \frac{(Z_A M_B^2 + Z_B M_A^2)}{M_A M_B (M_A + M_B)}, \quad (16)$$

where  $M_A$  and  $M_B$  are the masses of each nuclei in atomic mass units and  $Z_A$  and  $Z_B$  are the atomic number of each nuclei. It is important to take into account that the importance of the rotation of the electronic cloud can be decisive. For example, the calculated value for the nuclear contribution to the OH rotational  $g$ -factor is  $g_r^{\text{nuclear}} \simeq 5.25 \times 10^{-4}$  while the measured value is  $g_r = -6.33 \times 10^{-4}$  (Brown et al. 1978).

A simplification of the functional form of the Zeeman hamiltonian arises when the quantization axis  $z$  lies along the magnetic field direction. In this case, the scalar products between the magnetic field vector and the angular momentum operators in Eq. (14) are transformed into their corresponding projections along this axis multiplied by the modulus of the magnetic field vector. These projections are the spherical components of the operators along the  $z$  axis of the laboratory frame:

$$H_Z = g_S \mu_0 B \bar{S}_0^1 + g_L \mu_0 B \bar{L}_0^1 - g_r \mu_0 B (\bar{J}_0^1 - \bar{S}_0^1). \quad (17)$$

### 2.3. Matrix Elements

The energy levels of a diatomic molecule in the presence of an arbitrary magnetic field can be obtained via the numerical diagonalization of the total effective Hamiltonian matrix. In contrast to previous approaches, ours does not make use of any perturbational calculation since we diagonalize the full Hamiltonian including the Zeeman contribution. The first step is to write the effective Hamiltonian matrix in the chosen Hund's case (a) basis set. The advantage of this basis set is that the majority of the molecular fixed frame components of the angular momentum operators are diagonal in this basis, which largely simplifies the evaluation of the Hamiltonian matrix elements.

Of course, for problems where Hund’s case (a) is a good representation of the angular momentum coupling of the particular rotational level of the electronic level under consideration, the Hamiltonian will be highly diagonal. In general, the Hamiltonian will have a non-diagonal contribution that manifest deviations from the Hund’s case (a) coupling.

One of the easiest ways to calculate the matrix elements of the effective Hamiltonian is to substitute the rotational eigenfunctions by their explicit expressions in terms of the rotation matrices given by Eq. (2). The complex conjugate of the rotational eigenfunctions  $\langle J\Omega M|$  are obtained by taking the complex conjugate of the rotation matrix and transforming them with the help of the conjugation property given by Eq. (3). Since many of the matrix elements of the angular momentum operators are known in the molecular fixed frame, it is convenient to evaluate them in this frame. In case the components of a tensor in the laboratory frame appear in the Hamiltonian (for example in the Zeeman Hamiltonian), a transformation to the molecular fixed frame is performed using the standard transformation rules for the tensorial components given by Eq. (5). Finally, the calculation of the matrix elements of a spherical component of an arbitrary operator  $A_q^k$  is reduced to an integration over the Euler angles. The integrands of the  $\langle J'\Omega'M'|A_q^k|J\Omega M\rangle$  integrals consist in the product of two or three rotation matrices (two from the rotational eigenfunction and an extra one from the transformation to the molecular fixed frame). These integrals are easily calculated using the Weyl’s theorem given by Eq. (B1) and the property given by Eq. (B2) in Appendix B. In other cases, it is advantageous to directly use Wigner-Eckart’s theorem given by Eq. (6). For facilitating the calculation and the reproducibility of our results, we give the analytical expressions for the matrix elements of each term of the Hamiltonian in Appendix C.

## 2.4. Diagonalization

From an inspection of the explicit formulae for the matrix elements of the effective Hamiltonian in Appendix C, we can see that many of the terms included for the description of the diatomic molecule are diagonal in several quantum numbers. For instance, the Hamiltonian associated to the spin-orbit coupling is completely diagonal in Hund’s case (a) basis set. The molecular rotation contribution is diagonal in  $\Lambda$ ,  $S$ ,  $J$  and  $M$ , but not in<sup>1</sup>  $\Sigma$  and  $\Omega$ , while the Zeeman interaction is diagonal only in  $\Lambda$ ,  $S$  and  $M$ . Consequently, in the non-zero field case, the total angular momentum  $J$  is not a good quantum number. Therefore, only  $M$  remains as a good quantum number and the effect of the magnetic field has to be described in the Paschen-Back regime. Strictly speaking,  $J$  is not a good quantum number for any arbitrary value of the magnetic field strength. Obviously, for sufficiently weak magnetic fields,  $J$  is an approximately good quantum number and we can safely treat the molecule in the Zeeman regime.

---

<sup>1</sup>These are good quantum numbers in the case of a non-rotating molecule, but they are not good quantum numbers when rotation is taken into account.

When selecting the basis set, we have to make sure that the chosen set of  $|\Lambda S \Sigma; \Omega J M\rangle$  functions has to be complete enough to capture all the non-diagonal terms in the Hamiltonian matrix. In our case, the Hund’s case (a) basis set was chosen using the following rules:

- We include eigenfunctions with the two possible values of the projection of the orbital angular momentum on the internuclear axis  $\Lambda$ , i.e.,  $\pm\Lambda$ . This is fundamental to appropriately take into account the effect of  $\Lambda$ -doubling in which there is a break of the degeneracy between energy levels with the same value of  $|\Lambda|$ . Since in this paper we do not include any  $\Lambda$ -doubling interaction, the eigenvalues corresponding to both values of  $\Lambda$  are degenerate. However, if  $\Lambda$ -doubling needs to be explicitly accounted for, it is only a matter of including the appropriate effective Hamiltonian and calculating its matrix elements in Hund’s case (a) basis set.
- We include eigenfunctions with the two possible values of the projection of the spin on the internuclear axis  $\Sigma$ , i.e.,  $\pm\Sigma$ .
- When calculating the energy of the magnetic sublevels of a given level with total quantum number  $J$ , we also include the effect of the non-diagonal terms between the  $J$  level and the levels with  $J-1$  and  $J+1$ . This is only necessary when a magnetic field is present because the contribution of the Zeeman splitting is the only term included in the effective Hamiltonian which is non-diagonal in the quantum number  $J$ . In some cases (for instance, for heavy molecules), one may be interested in including non-diagonal terms with  $\Delta J = \pm 2$ . With the present approach, this is only a matter of augmenting the basis set by taking into account  $J-2$ ,  $J-1$ ,  $J$ ,  $J+1$  and  $J+2$  for a given level  $J$ .
- For each value of  $J$ , we include all the possible values of  $M$  from  $-J$  to  $J$ . It is important to note that the Hamiltonian is always diagonal in  $M$  unless the hyperfine structure is taken into account.

The total number of eigenfunctions included in the basis set and, consequently, the size of the effective Hamiltonian matrix, is obtained by summing all the possible values of the quantum numbers: 2 possible values of  $\Lambda$  (1 in case  $\Lambda = 0$ ),  $2S + 1$  possible values of  $\Sigma$  and  $2J + 1$  values of  $M$  for each included value of  $J$ . Therefore, the size of the basis set can be expressed in terms of the spin of the electronic state and the  $J$  value of the level of interest:

$$\mathcal{N} = \begin{cases} 3(2S + 1)(2J + 1) & \text{if } \Lambda = 0, J \geq 1 \\ 6(2S + 1)(2J + 1) & \text{if } \Lambda \neq 0, J \geq 1. \end{cases} \quad (18)$$

For instance, let us assume we choose a  ${}^2\Pi$  electronic state. The eigenfunctions of the form  $|\Lambda S \Sigma; \Omega J M\rangle$  used for the calculation of the energies of a rotational level  $J$  in this state are  $|1, 1/2, 1/2; 3/2, J', M\rangle$ ,  $|1, 1/2, -1/2; 1/2, J', M\rangle$ ,  $|-1, 1/2, 1/2; -1/2, J', M\rangle$  and  $|-1, 1/2, -1/2; -3/2, J', M\rangle$  (we have separated each number with commas for clarity reasons). Since we include the coupling for the values of  $J$  between  $J-1$  and  $J+1$ , we have to build such a set of eigenfunctions for each

value of  $J' = J - 1, J, J + 1$ . Additionally, we take into account the values of  $M$  for each allowed value of  $J'$  that are in the range  $-J'$  to  $J'$ . Summing up all the eigenfunctions obtained from the previous combinations, we end up with  $24J + 12$  eigenfunctions, a number which can be quite high even for small values of  $J$ .

The Hamiltonian matrix built with these eigenfunctions is a  $\mathcal{N} \times \mathcal{N}$  matrix. Due to the orthogonality properties of the eigenfunctions of Hund's case (a), many of the matrix elements are zero. As a result, the Hamiltonian matrix is very sparse (the number of non-zero elements is usually much less than the number of zero elements). In order to numerically diagonalize this matrix, we can make use of any of the available numerical procedures (see, e.g., Press et al. 1986), although algorithms specifically built for sparse matrices should be used in this case. As stated in Eq. (18), the size of the matrix increases linearly with the value of  $J$  and the calculation of the eigenvalues and eigenvectors of a big matrix represents a very hard numerical work even for intermediate values of  $J$ . However, we have seen that the effective Hamiltonian matrix is diagonal in the subspaces spanned by eigenfunctions with different values of  $M$  (or  $M_F$  in case we include the hyperfine structure). In this case, if we reorganize the matrix by ordering the basis set by their  $M$  quantum number, we end up with a block-diagonal matrix. Each block belongs to the space spanned by the eigenfunctions with a given value of  $M$ . Therefore, we transform the problem of diagonalizing a  $\mathcal{N} \times \mathcal{N}$  matrix to the diagonalization of  $2J + 1$  submatrices of size  $6(2S + 1)$ . This is shown in Figure 2, which corresponds to an example with  $J = 2$ . The standard algorithms applied to calculate the eigenvalues of a general matrix scale as  $\mathcal{O}(\mathcal{N}^3)$ , so that this reorganization translates into a huge decrease in the computing time (of the order of  $(2J + 1)^2$ ).

With the numerical diagonalization procedure, we calculate the eigenvalues and eigenvectors of the effective Hamiltonian matrix. The eigenvalues are associated to the energies of the magnetic sublevels  $M$  of a given rotational level of the electronic state of interest. The energy shift produced by the presence of a magnetic field can be obtained by the difference between these energies and the zero-field energies, obtained by diagonalization of the effective Hamiltonian neglecting the Zeeman Hamiltonian  $H_Z$ . The eigenvectors can be used then for calculating the expectation value of any operator. In our case, we are interested in calculating the expectation value of the dipolar moment operator, that is related to the relative strength of the transitions. The eigenfunction associated with any level can be written as the following linear combination of the eigenfunctions of Hund's case (a):

$$|\Psi\rangle = \sum_{\Lambda\Sigma\Omega J} c_{\Lambda\Sigma\Omega J} |\Lambda S \Sigma \Omega J M\rangle, \quad (19)$$

where the sum is extended over the values of  $\Lambda$ ,  $\Sigma$ ,  $\Omega$  and  $J$  included in the basis set. Since the matrix elements of the dipolar moment operator are known in Hund's case (a) (see, e.g., Schadee 1978), it is possible to use the previous linear combination to calculate it in the new basis.

### 3. Illustrative Results

This section is devoted to showing some comparisons between the results obtained via our numerical diagonalization of the Hamiltonian and with the previous approach to the molecular Zeeman effect based on Schadee’s (1978) theory. Although the formalism of Schadee (1978) allows one to calculate the Zeeman splittings and strengths of the Zeeman components of transitions among doublet states ( $S = 1/2$ ), it has been recently extended to transitions among states with arbitrary spins but for the linear Zeeman regime (Berdyugina & Solanki 2002). Our approach is suitable also for calculating the Zeeman splittings and strengths of the components for the case in which a transition to the Paschen-Back regime occurs for electronic states with arbitrary spins. The Hamiltonian diagonalization approach is the most general one, since it permits us to include easily any additional coupling among the angular momenta of the molecule and is valid for arbitrary strengths of the external field. Moreover, it can be applied to any electronic state with an arbitrary value of the spin.

Since one of the various applications we are carrying out is the synthesis of Stokes profiles induced by the molecular Zeeman effect in strongly magnetized regions of the solar atmosphere, we show first the Zeeman patterns for several lines of different diatomic species which are observed in the solar atmosphere. As is well known, a Zeeman pattern diagram shows the position and relative strength of each of the  $\sigma$  ( $\Delta M = \pm 1$ ) and  $\pi$  ( $\Delta M = 0$ ) components which arise from transitions among the magnetic sublevels of the upper and lower rotational levels of a given spectral line. The components in the upper part of the diagram are the  $\sigma$  components, with the  $\Delta M = -1$  transitions indicated as vertical lines going upwards and the  $\Delta M = 1$  transitions indicated as vertical lines going downwards. The relative strength of each component is proportional to the length of the vertical line. Additionally, the  $\pi$  components are in the lower part of the diagram. We have selected several molecular lines from MgH, OH, CN, C<sub>2</sub>, which show interesting Zeeman patterns (see, e.g., Schadee 1978; Illing 1981; Berdyugina & Solanki 2002; Asensio Ramos & Trujillo Bueno 2003; Asensio Ramos et al. 2005). In addition, we show also the Zeeman patterns for the CCS radical, which is a molecule of interest in the research field of star formation regions. Since this is a linear molecule, it can be described with the same formalism as if it were a diatomic molecule.

#### 3.1. Doublet states

##### 3.1.1. MgH

Our first example is the P<sub>2</sub>(5.5) line of the  $A^2\Pi - X^2\Sigma^+$  (0,0) electronic band of MgH. The ensuing MgH lines, which are located in the visible range around 5150 Å, have recently become of interest because, apart from presenting an interesting magnetic sensitivity, they show conspicuous scattering polarization signals when observed close to the solar limb (Stenflo & Keller 1996, 1997).

Figure 3 shows the Zeeman patterns obtained for a magnetic field strength of 1000 G. The

left panel concerns the results obtained using the theory developed by Schadee (1978) while the right panel shows the results obtained using our numerical diagonalization of the Hamiltonian. The molecular constants have been obtained from Huber & Herzberg (2003). For consistency with the assumptions of Schadee (1978) and in order to properly compare the results, we have included the very same terms in the effective Hamiltonian. In this case, the total Hamiltonian of the  $A^2\Pi$  electronic state has only contributions from the spin-orbit coupling, while that of the lower  $X^2\Sigma^+$  level has only contributions from the spin-rotation coupling. Figure 3 shows that both Zeeman patterns are indistinguishable, a proof that our numerical diagonalization technique is working properly. As previously indicated by Schadee (1978) (see also Berdyugina & Solanki 2002), such MgH lines present strong Paschen-Back effects. The reason is that the lower electronic state has a very small spin-rotation constant and the energy gap between two consecutive energy levels is very small. Therefore, the presence of a weak magnetic field leads to a Zeeman splitting comparable to this energy gap, which produces interferences between the magnetic substates. The presence of Paschen-Back effects produce a deformation of the Zeeman pattern with respect to the symmetric situation of the linear Zeeman regime. The ultimate cause of such interferences is that the Zeeman Hamiltonian  $H_Z$  is not diagonal in  $J$ , so that the energy levels do not have a  $J$  value associated with them. When a magnetic field is present each energy level has contributions from levels having different values of  $J$  in the zero-field case.

### 3.1.2. OH

The next two examples shown in Figures 4 and 5 are for the  $P_1(10.5)$  and  $P_2(9.5)$  near-IR lines of OH, which belong to the vibro-rotational (2,0) band of the fundamental electronic state  $X^2\Pi$ . Here the transition to the Paschen-Back regime occurs for magnetic strengths slightly below  $10^6$  G (Berdyugina & Solanki 2002). Therefore, for magnetic fields of  $\sim 1000$  G we are safely in the Zeeman regime. Similarly to the MgH case, the left panels show the results obtained with the theory of Schadee (1978), while the right panels show the results that we have obtained when using the numerical diagonalization of the Hamiltonian including only those terms which were considered by Schadee (1978). The molecular constants have been also obtained from Huber & Herzberg (2003). Note the extremely good agreement between both calculations. Since these OH lines are in an intermediate coupling scheme between Hund’s case (a) and (b) (Berdyugina & Solanki 2002), this calculation constitutes another proof that our numerical diagonalization technique is working properly. Although we have written the Hamiltonian matrix using the basis functions of Hund’s case (a), we can correctly recover the behavior for levels which are not correctly described under this case. In this situation, the Hamiltonian is non-diagonal and the final eigenfunctions result from appropriate combinations of the Hund’s case (a) eigenfunctions.

The circular polarization profiles produced by these OH lines in sunspot umbrae were first observed by Harvey (1985) and modeled by Berdyugina & Solanki (2001) taking into account that the effective Landé factor of the two lines have opposite signs (Rüedi et al. 1995). The fact that

both lines have effective Landé factors of opposite sign can be noted in Figs. 4 and 5. To this end, we recall the definition of the effective Landé factor as the wavelength shift from line center of the *center of gravity* of the  $\Delta M = -1$  components in Lorentz units (i.e., in units of  $\lambda_B = \lambda_0^2 \nu_L / c$ , where  $\lambda_0$  is the central wavelength,  $c$  is the speed of light and  $\nu_L$  is the Larmor frequency of the magnetic field). The Zeeman patterns show that the displacement from line center of the  $\Delta M = -1$  components have opposite signs for both lines.

With the polarization sensitivity we can obtain nowadays with the available solar polarimeters, the effective Hamiltonian we have used appears to be sufficient for the description of the OH transitions. However, we must emphasize that additional effects, like for instance the  $\Lambda$ -doubling, can be easily included in case a more realistic description turns out to be needed for explaining the emergent Stokes profiles.

### 3.1.3. CN lines in the IR

Another interesting example is the calculation of the Zeeman patterns for a molecular transition with high  $J$ -values, since it permits to test the numerical diagonalization approach for a case in which the effective Hamiltonian matrix is very large. One example is the  $Q_1(46.5)$  near-IR line of CN observed by Asensio Ramos et al. (2005). This line belongs to the  $A^2\Pi - X^2\Sigma^+$  electronic transition of CN and it is located in the same spectral region as the two OH lines discussed in the previous example. The rotational constants were again taken from Huber & Herzberg (2003). The magnetic field at which the transition to the Paschen-Back regime occurs for the levels of the upper  $A^2\Pi$  electronic state is  $\sim 560$  kG (e.g., Berdyugina & Solanki 2002). Therefore, we can safely treat them in the Zeeman regime for the typical stellar magnetic fields. However, the levels of the  $A^2\Pi$  electronic state have to be described in an intermediate coupling scheme between Hund’s cases (a) and (b). On the other hand, the levels of the lower electronic state  $X^2\Sigma^+$  can be correctly described under the Hund’s case (b) coupling when the magnetic field is weak enough so that we are in the linear Zeeman regime. However, the transition to the Paschen-Back regime in the lower electronic state occurs for rather weak fields ( $\sim 77$  G for the lowest  $J$  levels). For this reason, these lines are always in the Paschen-Back regime under the typical magnetic fields of sunspots. This example represents then a complicated problem in which neither the Zeeman regime nor any of the limiting Hund coupling cases can be applied.

Asensio Ramos et al. (2005) have pointed out that the observed polarization signal from this and other similar lines present an anomalous behavior, which is due to the peculiar form of the Zeeman patterns. In Fig. 6 we show the Zeeman patterns for this line calculated via the Hamiltonian diagonalization technique. We have verified that these results are similar to those obtained using the formulation of Schadee (1978). Figure 6 shows the patterns for weak fields (50 G), intermediate fields (500 and 2500 G) and very strong fields (30000 G). The first one shows that, even for weak fields, the CN lines cannot be correctly described under the Zeeman regime and that interferences between close  $J$  levels are of importance. At the typical kG field



strengths of sunspots, the  $\Delta M = \pm 1$  components have almost the same center of gravity while that of the  $\Delta M = 0$  components has a displacement with respect to the  $\Delta M = \pm 1$  components. This peculiarity, produced by the Paschen-Back regime, leads to the explanation of the anomalous emergent Stokes profiles in the umbral spectrum.

#### 3.1.4. CN lines in the UV

Another case of interest concerning transitions between doublet states is the  $B^2\Sigma^+ - X^2\Sigma^+$  ultraviolet transition of CN. This band has recently gained some attention due to the strong linear polarization signals observed close to the solar limb (Stenflo 2003, Gandorfer 2003). Theoretical investigations of the scattering polarization and the Hanle effect in these molecular lines have been carried out by Asensio Ramos & Trujillo Bueno (2003, 2005) in order to explain the *ladder* structure of the observed  $Q/I$  signals. Since the magnetic field in the observed *quiet* regions is assumed to be relatively weak and the scattering polarization calculations are very demanding, these theoretical investigations were performed by using the Landé factors obtained under Hund’s case (b) coupling.

Here we show that the Paschen-Back effect in this electronic system is of importance for fields of the order of 1000 G (and even for fields below 100 G). The rotational constants were taken from Huber & Herzberg (2003). We have plotted only the results obtained via the numerical diagonalization of the total Hamiltonian, but they are similar to those obtained using the formulae of Schadee (1978). Figure 7 shows the Zeeman patterns for the  $R_1(70.5)$  line for a field strength of 1000 G. This result is representative of the Paschen-Back effect for lines between high  $J$  levels. The  $R_1(70.5)$  line is one of the spectral lines presenting strong scattering polarization signals in the spectral region between 3771 Å and 3775 Å. It is interesting to note that Paschen-Back effects are important for fields as low as 1000 G for transitions between high- and low- $J$  levels. Therefore, for the typical kG fields of sunspot umbrae the lines of this system should present anomalous Stokes profiles. The observable effects of these perturbed Zeeman patterns on the emergent Stokes profiles should be similar to those observed in the lines of the  $A^2\Pi - X^2\Sigma^+$  system, and whose Zeeman patterns are shown in Figure 6.

### 3.2. Non-doublet states

#### 3.2.1. $C_2$

The first case we have considered is the (0,0) transition of the electronic band  $d^3\Pi - a^3\Pi$  of  $C_2$ ; i.e., one of the so-called Swan band. The investigation of this band in the solar atmosphere has gained some interest recently due to the linear polarization signals produced by scattering processes (see, e.g., Gandorfer’s 2000 atlas of the linearly-polarized solar limb spectrum) and their sensitivity to the presence of a weak magnetic field via the Hanle effect (e.g., Trujillo Bueno et al. 2004). In

this paper we are however interested in calculating the Zeeman patterns of some lines of this band for a magnetic field of 3000 G. We have chosen the  $P_1(7)$  and  $P_2(6)$  lines as representative of the results which can be obtained also for other lines of the Swan system. The results we have obtained via our numerical diagonalization of the total Hamiltonian are shown in Figure 8.

The critical magnetic field at which one starts to detect signatures of the transition to the Paschen-Back regime for this electronic system is larger than 70000 G (Berdyugina & Solanki 2002). Since we are interested in much weaker fields, the magnetic sensitivity of the lines of this transition can be safely modeled in the Zeeman regime. This can also be inferred from the very symmetric appearance of the Zeeman patterns shown in Figure 8. Furthermore, the deviations from Hund’s case (b) are not very large and we have verified that the obtained Zeeman patterns have some similarities with those obtained in Hund’s case (b). An important conclusion regarding the effective Landé factor can be obtained by a quick look to the Zeeman patterns. Note that the center of gravity of the  $\Delta M = -1$  transition is very close to zero in the  $P_2(6)$  line while it is much larger for the  $P_1(7)$  line. This shows that the  $P_1$  lines are much more magnetically sensitive than the  $P_2$  lines. The same is valid for the  $P_3$  lines.

It is very difficult to find molecules having electronic states with  $S \neq 1/2$  that present strong Paschen-Back effects and which can be observed in solar and/or stellar spectra in the visible and infrared regions. The target molecular transitions are those in which the energy difference between consecutive levels is small enough so that the Zeeman splitting for typical stellar magnetic fields produce significant interferences between levels with consecutive values of  $J$ . Since the spin-orbit coupling is usually much larger than the spin-rotation one (see Huber & Herzberg 2003 for the molecular constants), a candidate molecule should ideally have an electronic state with  $\Lambda = 0$  so that the small spin-rotation coupling gives strong interferences between closely lying energy levels. A few molecules observed in the solar and other stellar atmospheres present such states. This is the case of CO with its  $a^3\Sigma^+$  electronic state, which is radiatively linked with the fundamental  $X^1\Sigma^+$  level by a forbidden transition around 1800 Å.

Another case of interest is  $C_2$ , with the Ballik-Ramsay system. This system results from the electronic transition  $b^3\Sigma_g^- - a^3\Pi_u$  situated in the infrared (Ballik & Ramsay 1963), with the center of the band around 1.8  $\mu\text{m}$ . As an example, we show in Figure 9 the Zeeman patterns for the  $R_1(16)$  and  $P_1(16)$  lines. Both lines present strong Paschen-Back effects. Curiously, the deformed Zeeman patterns resemble those patterns we calculated for the CN lines of the  $A^2\Pi - X^2\Sigma^+$  system. In fact, we expect that such  $C_2$  lines present Stokes profiles that resemble those observed in sunspot umbrae for the previously considered CN lines. Thus, they would present very weak circular polarization signals and stronger and antisymmetric linear polarization signals. Such  $C_2$  transitions can be easily observed in carbon stars (Goorvitch 1990) and they have been also detected in comets (Johnson & Larson 1983). In this respect, it is of interest to mention that Johnson & Larson (1983) give a list of possible observable bands in comets. The (0,0) band is around 5632.7  $\text{cm}^{-1}$ , the (1-0) band is around 7080.8  $\text{cm}^{-1}$  and the (2-0) band is around 8506.5  $\text{cm}^{-1}$ .

### 3.2.2. *SO and CCS*

Turning now our attention to the millimeter-wave region, it is worthwhile to mention that it is possible to observe pure rotational transitions in the lower rotational levels of molecules with ground electronic states having  $\Lambda = 0$  and  $S \neq 1/2$ . Some of these molecules are present in regions of star formation and the investigation of the Zeeman effect in these molecules is very important for gaining information about the magnetic field. This is the case of SO and the CCS radical, which are used as tracers of dense cores in star formation regions. Since they present no hyperfine structure, and due to the observed narrow and intense emission peaks, they have been used to measure the velocity structure in dense cores (Langer et al. 1995). Due to the two unpaired electrons present in both molecules, the Zeeman splittings are important, and this fact has been used for searching for magnetic fields in the densest parts of star formation regions. Shinnaga & Yamamoto (2000) have calculated the Zeeman effect in the  $^3\Sigma^-$  fundamental electronic state of both SO and CCS in order to give accurate Landé factors for several rotational lines. Figure 10 demonstrates that we are able to reproduce their Fig. 2 for the  $R_1(3)$  transition of CCS. Of course, we have used the same rotational and coupling constants in order to be able to compare properly both results. The results of Shinnaga & Yamamoto (2000) were obtained by diagonalization of the effective Hamiltonian written using Hund’s case (b) eigenfunctions. In this case, it is more appropriate because, for weak rotation, the angular momenta coupling is closer to Hund’s case (b). Remarkably, using our approach based on Hund’s case (a) eigenfunctions, we obtain the same results, thus demonstrating again that our approach is very robust. Interestingly, we find that we need to use a magnetic field strength of 1 mG instead of 100  $\mu$ G in order to reproduce their results. Apparently, the magnetic field indicated in the labels of Fig. 2 in Shinnaga & Yamamoto (2000) appears to be inconsistent with the results given in the text, that are otherwise correct. Finally, it is important to note that, since the energy separation of rotational levels decreases as the weight of the molecule increases, it might be possible that the  $\Delta J = \pm 2$  matrix-elements are non-negligible for a correct modeling of the Zeeman splitting in some molecular species.

## 4. Conclusions

The numerical approach presented in this paper allows us to calculate the effect of a magnetic field on the energy levels of diatomic molecules for arbitrary values of the total electronic spin and of the magnetic field strength (i.e., it is valid for states of any multiplicity and for both the Zeeman and incomplete Paschen-Back regimes). The ensuing computer program we have developed gives the splittings of the molecular energy levels and the strengths of the individual Zeeman components (i.e., the Zeeman patterns of molecular transitions), which is the basic information we use in our radiative transfer code for modeling the emergent Stokes parameters from magnetized stellar atmospheres. It is based on an efficient numerical diagonalization of the effective Hamiltonian, which gives the eigenvalues and eigenvectors for each magnetic sublevel, from where we obtain the energies of the molecular levels and the expectation values of the dipole moment operator between

the pair of levels producing the molecular transition under consideration.

Our numerical diagonalization approach of the effective Hamiltonian can treat cases in which quantum interferences between very close in energy levels lead to the transition to the Paschen-Back regime. We take into account the effect of non-diagonal terms between levels with  $\Delta J = \pm 1$  in a self-consistent way, without making use of any perturbative calculation. Our strategy generalizes previous ones which only allowed the investigation of doublet states for arbitrary values of the magnetic field (Schadee 1978) or states with arbitrary spin but in the linear Zeeman regime (Berdyugina & Solanki 2002). Additionally, our computer program allows a straightforward inclusion of any additional term into the effective Hamiltonian, so that the description of the molecular motion can be as refined as needed.

We have performed several comparisons between our results and those obtained via previous formulations based on Schadee’s (1978) theory, demonstrating that both results are indistinguishable when the very same terms of the effective Hamiltonian are included. We have also performed calculations for several molecular transitions arising from non-doublet states (e.g., states with  $S = 1$ ). Since the theory developed by Schadee (1978) is limited to doublet states, we have performed comparisons in the Zeeman regime with the results given by pure Hund’s coupling cases. Furthermore, we have also calculated Zeeman patterns for diatomic lines in triplet states in which clear Paschen-Back effects are at work.

It has been clearly shown in physics laboratory experiments that a very detailed description of the molecular motion is needed to investigate correctly the magnetic properties of diatomic molecular lines (e.g., Brown & Carrington 2003, and references therein). However, in astrophysics the investigation and application of the Zeeman and Hanle effects in molecular lines is still at an early stage of development. Fortunately, a new generation of polarimeters and telescopes should allow us to obtain high-quality spectropolarimetric observations with unprecedented spectral resolution and polarimetric sensitivity. We believe that the numerical diagonalization approach described in this paper constitutes the ideal framework to investigate in detail the magnetic properties of molecular lines in different astrophysical environments, since it permits a rather straightforward inclusion of all the desired terms in the effective Hamiltonian. Among the various investigations we have in mind for the near future, we would like to mention the influence of the hyperfine structure and/or the  $\Lambda$ -doubling on both the Zeeman and Hanle effects in the spectral lines of diatomic molecules.

We thank Egidio Landi Degl’Innocenti and the anonymous referee for their careful reading of our paper and for suggesting some useful improvements. This research has been funded by the European Commission through the Solar Magnetism Network (contract HPRN-CT-2002-00313) and by the Spanish Ministerio de Educación y Ciencia through project AYA2004-05792.

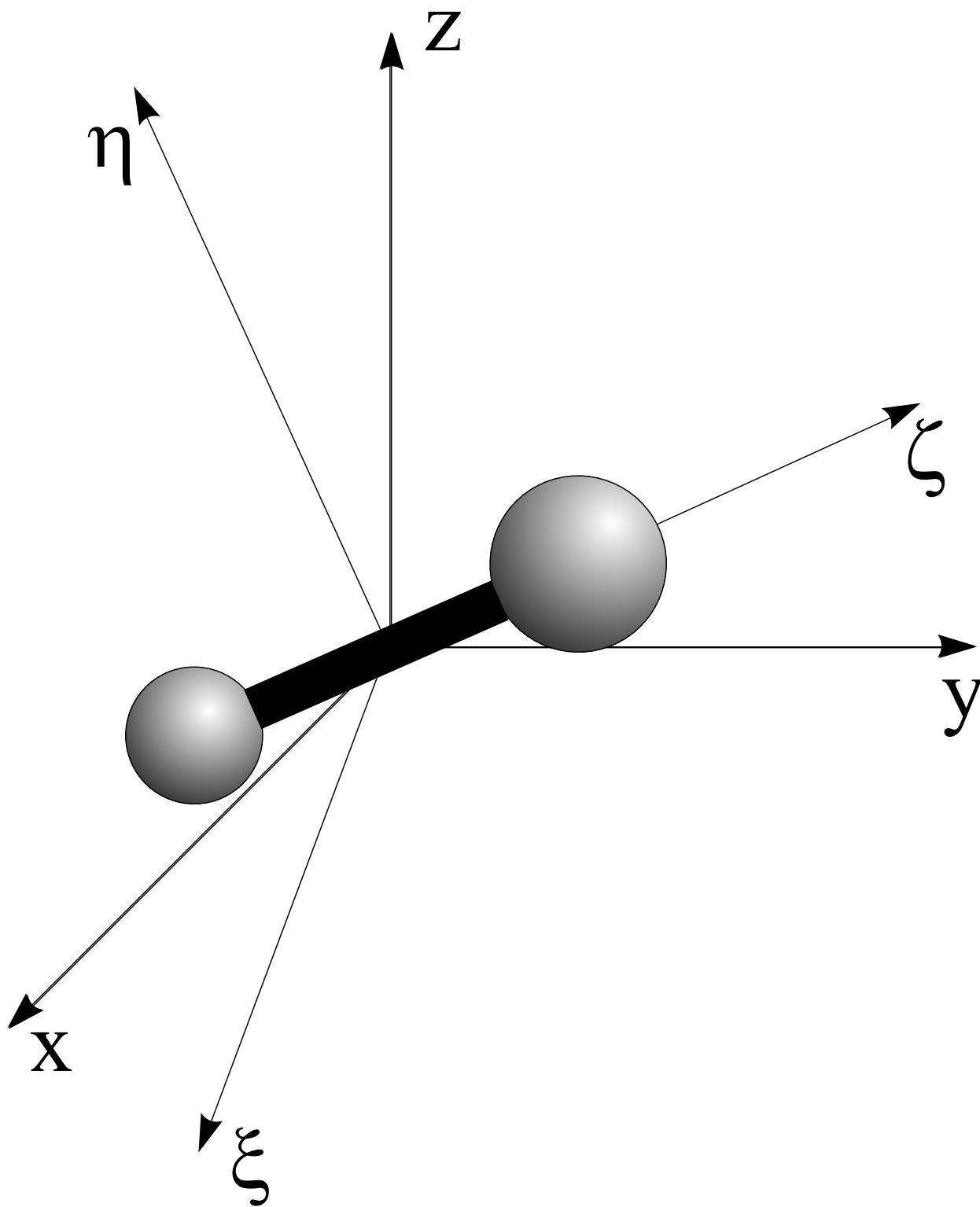


Fig. 1.— The two frames used to describe the motion of a diatomic molecule. The  $F$  frame with axes  $(x, y, z)$  is fixed at the center of mass of the molecule, with the  $z$  axis along the quantization axis. The  $F'$  frame with axes  $(\xi, \eta, \zeta)$  rotates with the molecule, with the  $\zeta$  axis along the internuclear axis. The transformation of any tensorial quantity between both frames can be easily carried out with the aid of Eqs. (4) and (5).

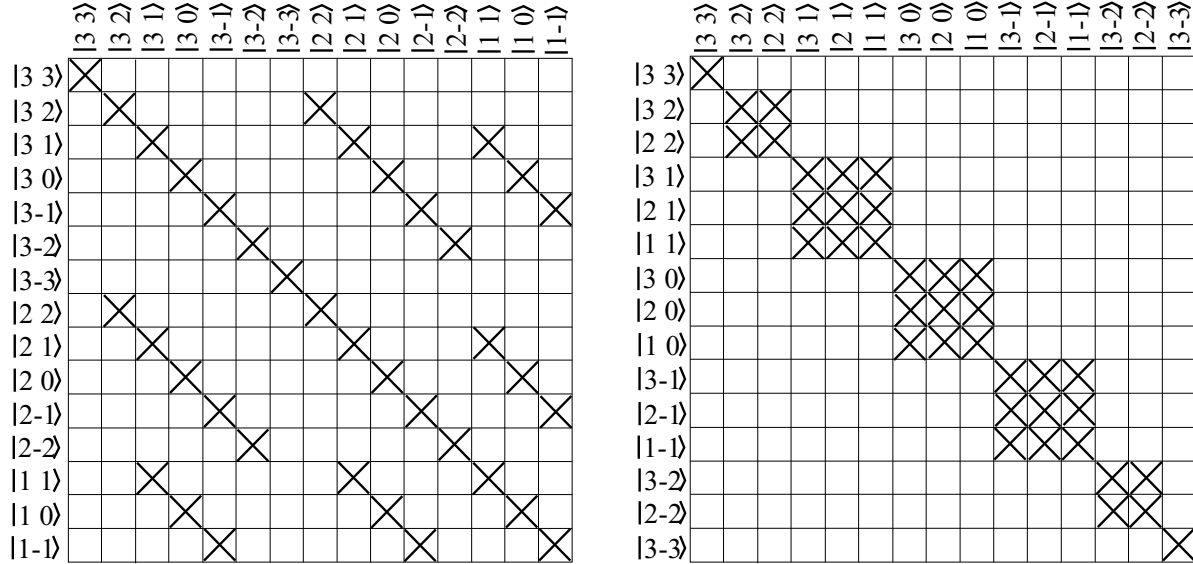


Fig. 2.— Rotational part of the effective Hamiltonian matrix for a level with  $J = 2$ . A similar matrix has to be built for any combination of  $\Lambda$  and  $\Sigma$ . We indicate with a “ $\times$ ” the elements which can, in principle, be different from zero. The rest of matrix elements are zero due to the orthonormality of the eigenfunctions. Since we are indicating only the rotational part of the Hamiltonian, the eigenfunctions are of the form  $|JM\rangle$ , with  $\Omega$  prescribed by the values of  $\Lambda$  and  $\Sigma$ . The left panel shows the Hamiltonian matrix when the basis set is sorted by the value of  $J$ , that results in a highly non-diagonal matrix. The right panel shows the same Hamiltonian matrix when the basis set is ordered by the value of  $M$ . Since the effective Hamiltonian is diagonal in the  $M$  quantum number, the resulting matrix is block-diagonal, thus allowing a block diagonalization in each of the subspaces spanned by the eigenfunctions with the same value of  $M$ .

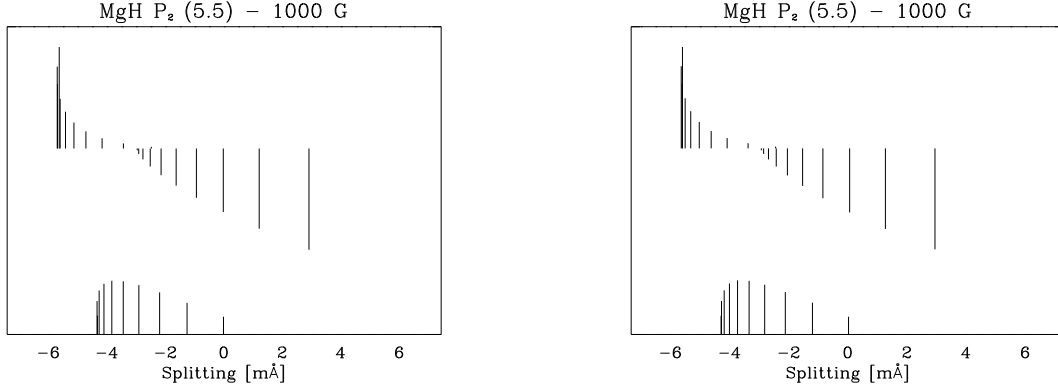


Fig. 3.— Zeeman patterns for a magnetic field strength of 1000 G for the  $P_2(5.5)$  line of the MgH electronic transition  $A^2\Pi - X^2\Sigma^+$ . The left panel shows the results applying the theory developed by Schadee (1978) while the right panel shows those obtained from the numerical diagonalization of the Hamiltonian. This low- $J$  transition of MgH is in the transition to the Paschen-Back regime for a field of 1000 G, thus the Zeeman patterns are highly perturbed due to the presence of the non-diagonal  $\Delta J = \pm 1$  terms in the total effective Hamiltonian.

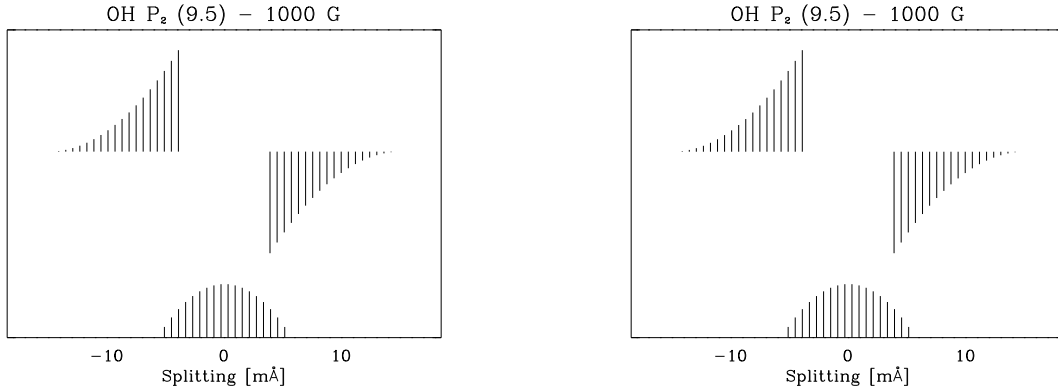


Fig. 4.— Zeeman patterns for a magnetic field strength of 1000 G for the  $P_2(9.5)$  line between vibrational levels of the fundamental  $X^2\Pi$  state of OH. The left panel shows the results applying the theory developed by Schadee (1978) while the right panel shows those obtained from the numerical diagonalization of the Hamiltonian. The magnetic field at which there are interactions between adjacent rotational levels in this electronic state is much higher than 1000 G, so that this line is in the Zeeman regime. As a consequence, the Zeeman patterns are almost unperturbed. However, the transition has to be described using an intermediate coupling between Hund’s cases (a) and (b).

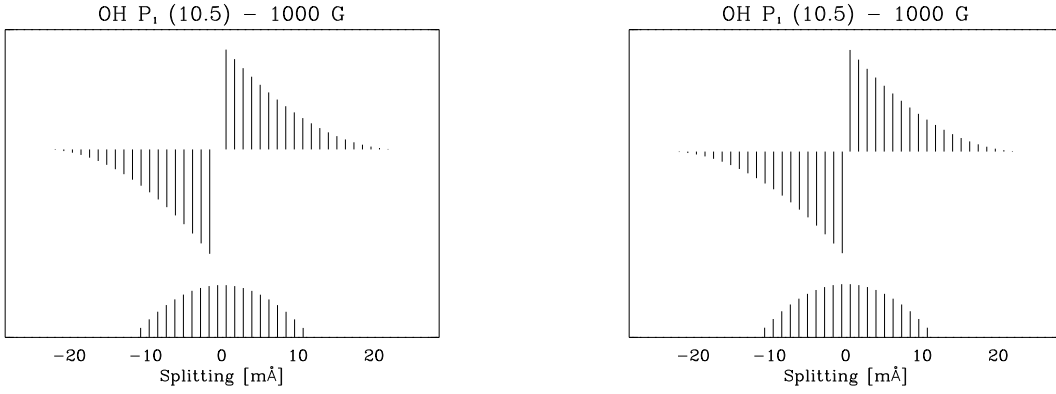


Fig. 5.— Same as Figure 4 but for the  $P_1(10.5)$  line between vibrational levels of the fundamental  $X^2\Pi$  state of OH.

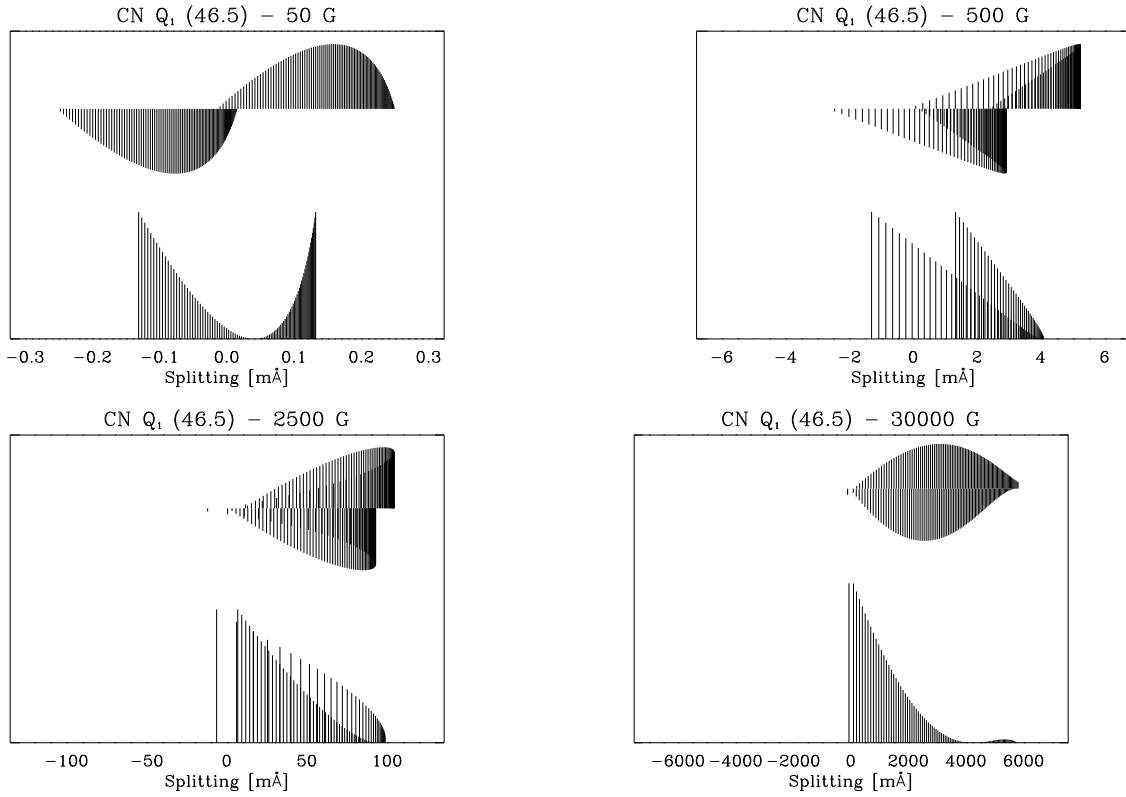


Fig. 6.— Zeeman patterns for 50, 500, 2500 and 30000 G of the  $Q_1(46.5)$  CN line. Note that the  $\sigma$  and  $\pi$  components tend to be symmetric for low fields and get deformed due to the transition to the Paschen-Back regime. At very high fields, the symmetry is again recovered. This is an example of a transition in which the  $\Delta J = \pm 1$  matrix elements in the effective Hamiltonian are non-zero even for fields as low as 50 G.



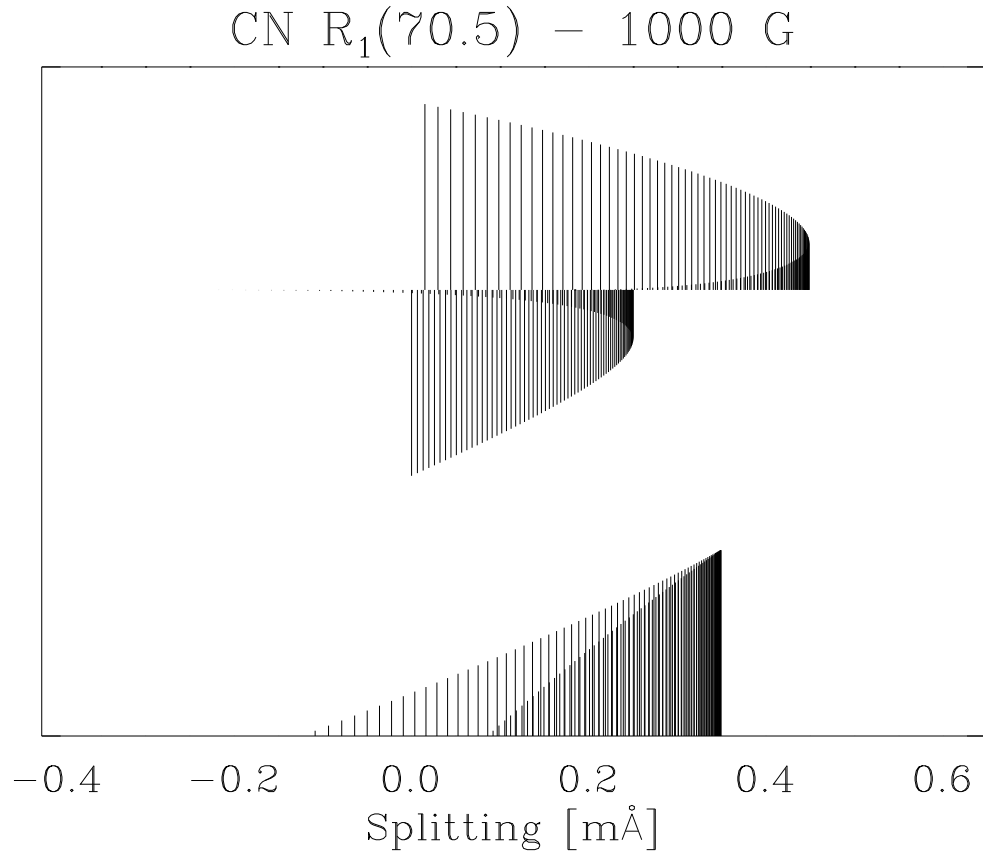


Fig. 7.— Zeeman patterns for a magnetic field strength of 1000 G for the  $R_1(70.5)$  line of the ultraviolet electronic transition  $B^2\Sigma^+ - X^2\Sigma^+$  of CN. Note that the Paschen-Back effect is present even for high  $J$  values.

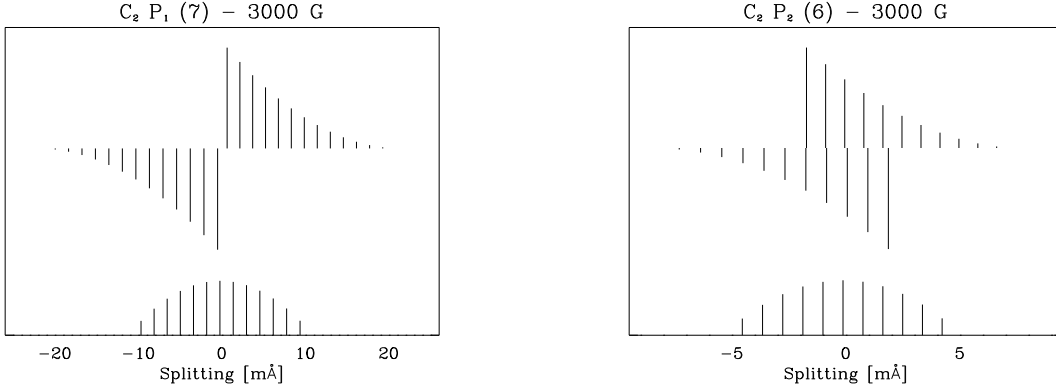


Fig. 8.— Zeeman patterns for a magnetic field strength of 3000 G for the  $P_1(7)$  and  $P_2(6)$  lines of the electronic transition  $d^3\Pi - a^3\Pi$  of  $C_2$ . In this case, since  $S = 1$ , the theory of Schadee (1978) cannot be applied and these results have been obtained with the numerical diagonalization of the Hamiltonian.

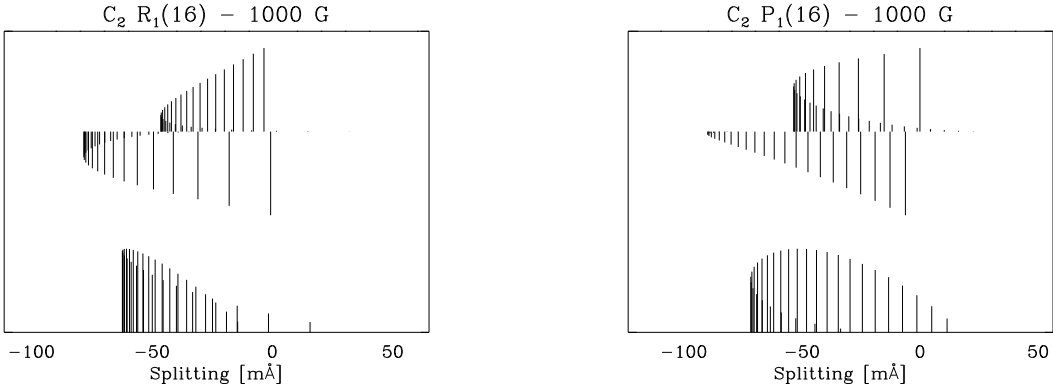


Fig. 9.— Zeeman patterns for a magnetic field strength of 1000 G for the  $R_1(16)$  and  $P_1(16)$  lines of the electronic transition  $b^3\Sigma_g^+ - a^3\Pi_u$  of  $C_2$  (the Ballik-Ramsay system). This is an example of a transition in which one of the levels has  $S \neq 1/2$  while having  $\Lambda = 0$ . Since the energy separation of the multiplet levels is small, the  $\Delta J = \pm 1$  matrix elements of the effective Hamiltonian are of importance because the splitting for moderate magnetic fields are of the order of the energy separation. The Zeeman patterns clearly show this perturbation in the transition to the Paschen-Back regime.

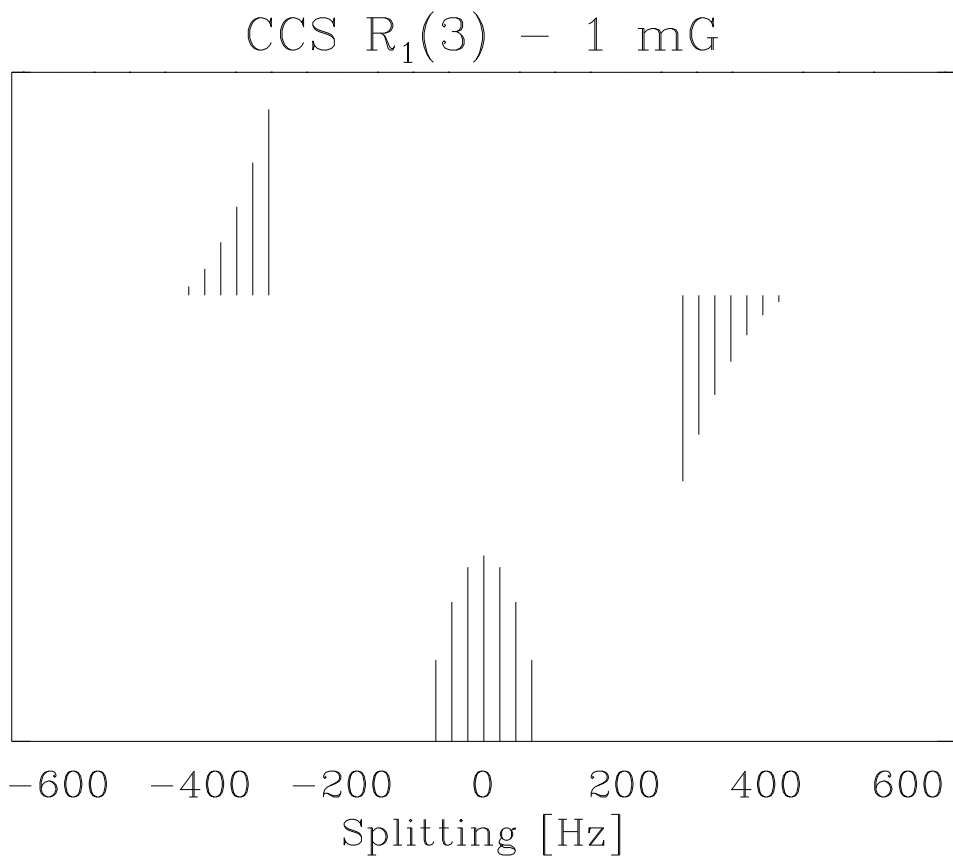


Fig. 10.— Zeeman patterns for a magnetic field strength of 1 mG for the  $R_1(3)$  pure rotational line of CCS in the fundamental  $^3\Sigma^-$  electronic state. This line has to be described in an intermediate coupling case between Hund’s case (a) and (b). The comparison with the results of Shinnaga & Yamamoto (2000) indicate that our approach based on a Hund’s case (a) basis set works for transitions which are almost perfectly described under a pure Hund’s case (b) coupling.

Hund's case	Case (a)	Case (b)
Good quantum numbers	$\Lambda, S, J, \Sigma$ ( $\Omega = \Lambda + \Sigma$ )	$\Lambda, S, J, N$
Degeneracy (non-rotating)	$\begin{cases} 2 & \text{if } \Lambda \neq 0 \\ 1 & \text{if } \Lambda = 0 \end{cases}$	$\begin{cases} 2(2S + 1) & \text{if } \Lambda \neq 0 \\ 2S + 1 & \text{if } \Lambda = 0 \end{cases}$
Degeneracy (rotating)	$\begin{cases} 2 & \text{if } \Lambda \neq 0 \\ 1 & \text{if } \Lambda = 0 \end{cases}$	$\begin{cases} 2 & \text{if } \Lambda \neq 0 \\ 1 & \text{if } \Lambda = 0 \end{cases}$
Values of $J$	$ \Omega ,  \Omega  + 1,  \Omega  + 2, \dots$	$ N - S ,  N - S  + 1, \dots, N + S$
Values of $N$	Not defined	$\Lambda, \Lambda + 1, \dots$
Conditions	$A\Lambda \gg BJ$	$A\Lambda \ll BJ$

Table 1: Brief description of Hund's cases properties.

### A. Hund's cases

This Appendix describes briefly the most common angular momentum coupling cases present in diatomic molecules. All angular momentum vectors of the molecule (electronic orbital  $\mathbf{L}$ , spin angular momentum  $\mathbf{S}$  and rotational angular momentum  $\mathbf{R}$ ) form a resultant total angular momentum which is designated by  $\mathbf{J}$ . Hund's coupling cases are distinguished by the strength of the coupling among all angular momenta present in the molecule.

In Hund's case (a), illustrated in the left panel of Figure 11, the orbital angular momentum is strongly coupled to the internuclear axis by electrostatic forces. The spin angular momentum is in turn strongly coupled to the orbital angular momentum through spin-orbit coupling. Additionally, the rotational motion is weakly interacting with the spin and orbital motions. In this case, the projection of the total electronic angular momentum  $\mathbf{\Omega}$  is well defined and composed of the projection of the orbital angular momentum  $\mathbf{L}$  on the internuclear axis ( $\Lambda$ ) plus the projection of the spin angular momentum  $\mathbf{S}$  on the internuclear axis ( $\Sigma$ ). The rotational angular momentum  $\mathbf{R}$  thus couples with the angular momentum along the internuclear axis  $\mathbf{\Omega}$  to form the total angular momentum  $\mathbf{J}$ . The condition for the suitability of Hund's case (a) is that the spin-orbit coupling  $A\Lambda\Sigma$  has to be much larger than  $BJ(J + 1)$ , with  $B$  the rotational constant and  $A$  the spin-orbit coupling constant.

In Hund's case (b), illustrated in the right panel of Figure 11, the spin angular momentum  $\mathbf{S}$  is very weakly coupled to the internuclear axis. In this case, the orbital angular momentum  $\mathbf{L}$  is still strongly coupled to the internuclear axis with projection  $\Lambda$ . Because of the weak coupling between the spin and the internuclear axis, it is not possible to define  $\mathbf{\Omega}$ . The vector  $\mathbf{\Lambda}$  couples then to the rotational angular momentum  $\mathbf{R}$  to form the resultant  $\mathbf{N}$  (the total angular momentum apart from spin). Finally, the angular momentum  $\mathbf{N}$  couples with the spin  $\mathbf{S}$  to form the total angular momentum  $\mathbf{J}$ . The condition under which Hund's case (b) applies is that the spin-orbit coupling must be much smaller than  $BJ(J + 1)$ .

Table 1 gives a summary of the good quantum numbers in both Hund's cases (a) and (b), together with information on the degeneracy of the levels in the rotating and non-rotating molecule. We also give the possible values of  $J$  and  $N$  (if defined) and the conditions under which each Hund's

case applies.

### B. Useful properties of the rotation matrices

This appendix gives some important and useful properties of the rotation matrices which can be found also in angular momentum books (see, e.g., Edmonds 1960, Brink & Satchler 1968, Judd 1975). Two properties are used for deriving the matrix elements of the Hamiltonian. The first one is the Weyl's theorem, which states that the integral of the product of three rotational matrices over the Euler angles can be easily calculated as follows:

$$\begin{aligned} \int_0^{2\pi} d\alpha \int_0^\pi d\gamma \int_0^{2\pi} d\beta \sin\beta \mathcal{D}_{M_1\Omega_1}^{J_1}(\alpha, \beta, \gamma) \mathcal{D}_{M_2\Omega_2}^{J_2}(\alpha, \beta, \gamma) \mathcal{D}_{M_3\Omega_3}^{J_3}(\alpha, \beta, \gamma) = \\ = 8\pi^2 \begin{pmatrix} J_1 & J_2 & J_3 \\ M_1 & M_2 & M_3 \end{pmatrix} \begin{pmatrix} J_1 & J_2 & J_3 \\ \Omega_1 & \Omega_2 & \Omega_3 \end{pmatrix}, \end{aligned} \quad (\text{B1})$$

where we have introduced the 3-j symbols according to their standard definition (see, e.g., Edmonds 1960). The other property of interest is

$$\begin{aligned} \int_0^{2\pi} d\alpha \int_0^\pi d\gamma \int_0^{2\pi} d\beta \sin\beta \mathcal{D}_{M_1\Omega_1}^{J_1}(\alpha, \beta, \gamma)^* \mathcal{D}_{M_2\Omega_2}^{J_2}(\alpha, \beta, \gamma) = \\ = \frac{8\pi^2}{2J+1} \delta_{J_1 J_2} \delta_{M_1 M_2} \delta_{\Omega_1 \Omega_2}, \end{aligned} \quad (\text{B2})$$

where  $\delta_{ab}$  is the Kronecker's delta, which is 1 for  $a = b$  and zero otherwise.

### C. Matrix elements of the effective Hamiltonian

This appendix gives the explicit form of the matrix elements of the effective Hamiltonian in Hund's case (a) basis set. One of the purposes is to show the explicit form of the matrix elements in order to recognize whether or not a contribution to the total Hamiltonian is diagonal in Hund's case (a) basis set. As it is mentioned in this paper, these expressions have been obtained by applying the Wigner-Eckart theorem to evaluate the tensorial form of the effective Hamiltonian given in Section 2.2, together with an extensive use of Racah's algebra and the properties outlined in Appendix B (see Brown & Carrington 2003 for details). If any of the terms is not diagonal in one of the quantum numbers of Hund's case (a) basis functions, we indicate it by using primed and non-primed quantities for the bra and the ket of the matrix element, respectively. For instance, the rotational Hamiltonian given by Eq. (C3) is diagonal in  $\Lambda$ ,  $S$ ,  $J$  and  $M$ , but not in  $\Sigma$  and  $\Omega$ .

### C.1. Spin-orbit coupling Hamiltonian

$$\langle \Lambda S \Sigma \Omega J M | H_{\text{SO}} | \Lambda S \Sigma \Omega J M \rangle = A \Lambda \Sigma + A_D \Lambda \Sigma [J(J+1) - \Omega^2 + S(S+1) - \Sigma^2], \quad (\text{C1})$$

### C.2. Spin-spin coupling Hamiltonian

$$\langle \Lambda S \Sigma \Omega J M | H_{\text{SS}} | \Lambda S \Sigma \Omega J M \rangle = \frac{2}{3} \lambda [3\Sigma^2 - S(S+1)], \quad (\text{C2})$$

### C.3. Rotational Hamiltonian

$$\begin{aligned} \langle \Lambda S \Sigma' \Omega' J M | H_{\text{rot}} | \Lambda S \Sigma \Omega J M \rangle &= B \delta_{\Sigma' \Sigma} \delta_{\Omega' \Omega} [J(J+1) - \Omega^2 + S(S+1) - \Sigma^2] \\ &\quad - 2B \sum_{q=\pm 1} (-1)^{J-\Omega'+S-\Sigma'} \begin{pmatrix} J & 1 & J \\ -\Omega' & q & \Omega \end{pmatrix} \begin{pmatrix} S & 1 & S \\ -\Sigma' & q & \Sigma \end{pmatrix} \\ &\quad \times \sqrt{J(J+1)(2J+1)S(S+1)(2S+1)}. \end{aligned} \quad (\text{C3})$$

### C.4. Centrifugal distortion Hamiltonian of order 4

$$\begin{aligned} \langle \Lambda S \Sigma' \Omega' J M | H_{\text{cd}}^{(4)} | \Lambda S \Sigma \Omega J M \rangle &= -D \delta_{\Sigma' \Sigma} \delta_{\Omega' \Omega} [J(J+1) - \Omega^2 + S(S+1) - \Sigma^2]^2 \\ &\quad + 4D \delta_{\Sigma' \Sigma} \delta_{\Omega' \Omega} \sum_{q=\pm 1} \sum_{\Omega'' \Sigma''} \begin{pmatrix} J & 1 & J \\ -\Omega & q & \Omega'' \end{pmatrix}^2 \begin{pmatrix} S & 1 & S \\ -\Sigma & q & \Sigma'' \end{pmatrix}^2 \\ &\quad \times J(J+1)(2J+1)S(S+1)(2S+1) - 2D \sum_{q=\pm 1} (-1)^{J-\Omega'+S-\Sigma'} \\ &\quad \times \begin{pmatrix} J & 1 & J \\ -\Omega' & q & \Omega \end{pmatrix} \begin{pmatrix} S & 1 & S \\ -\Sigma' & q & \Sigma \end{pmatrix} \sqrt{J(J+1)(2J+1)S(S+1)(2S+1)} \\ &\quad \times [2J(J+1) - \Omega^2 - (\Omega')^2 + 2S(S+1) - \Sigma^2 - (\Sigma')^2]. \end{aligned} \quad (\text{C4})$$

### C.5. Centrifugal distortion Hamiltonian of order 6

$$\langle \Lambda S \Sigma' \Omega' J M | H_{\text{cd}}^{(6)} | \Lambda S \Sigma \Omega J M \rangle = H \delta_{\Sigma' \Sigma} \delta_{\Omega' \Omega} [J(J+1) - \Omega^2 + S(S+1) - \Sigma^2]^3$$

$$\begin{aligned}
& +4H\delta_{\Sigma'\Sigma}\delta_{\Omega'\Omega}\sum_{q=\pm 1}\sum_{\Omega''\Sigma''}\begin{pmatrix} J & 1 & J \\ -\Omega & q & \Omega'' \end{pmatrix}^2\begin{pmatrix} S & 1 & S \\ -\Sigma & q & \Sigma'' \end{pmatrix}^2 \\
& \times J(J+1)(2J+1)S(S+1)(2S+1)[3J(J+1)-2\Omega^2-(\Omega'')^2+3S(S+1)-2\Sigma^2-(\Sigma'')^2] \\
& -2H\sum_{q=\pm 1}(-1)^{J-\Omega'+S-\Sigma'}\begin{pmatrix} J & 1 & J \\ -\Omega' & q & \Omega \end{pmatrix}\begin{pmatrix} S & 1 & S \\ -\Sigma' & q & \Sigma \end{pmatrix} \\
& \times\sqrt{J(J+1)(2J+1)S(S+1)(2S+1)}\left[[J(J+1)-\Omega^2+S(S+1)-\Sigma^2]^2\right. \\
& \quad \left.+[J(J+1)-(\Omega')^2+S(S+1)-(\Sigma')^2]^2\right. \\
& \quad \left.+[J(J+1)-\Omega^2+S(S+1)-\Sigma^2][J(J+1)-(\Omega')^2+S(S+1)-(\Sigma')^2]\right] \\
& +4\begin{pmatrix} J & 1 & J \\ -\Omega' & q & \Omega \end{pmatrix}^2\begin{pmatrix} S & 1 & S \\ -\Sigma' & q & \Sigma \end{pmatrix}^2J(J+1)(2J+1)S(S+1)(2S+1)\left] \quad (C5)
\end{aligned}$$

### C.6. Spin-rotation interaction Hamiltonian

$$\begin{aligned}
\langle \Lambda\Sigma\Sigma'\Omega'JM|H_{\text{sr}}|\Lambda\Sigma\Sigma\Omega JM\rangle & = \gamma\delta_{\Sigma'\Sigma}\delta_{\Omega'\Omega}[\Omega\Sigma-S(S+1)]+\gamma\sum_{q=\pm 1}(-1)^{J-\Omega'+S-\Sigma'} \\
& \times\begin{pmatrix} J & 1 & J \\ -\Omega' & q & \Omega \end{pmatrix}\begin{pmatrix} S & 1 & S \\ -\Sigma' & q & \Sigma \end{pmatrix}\sqrt{J(J+1)(2J+1)S(S+1)(2S+1)} \quad (C6)
\end{aligned}$$

### C.7. Zeeman Hamiltonian

$$\begin{aligned}
\langle \Lambda\Sigma\Sigma'J'M_J\Omega'|H_Z|\Lambda\Sigma\Sigma JM_J\Omega\rangle & = \mu_B B_0\sum_{q=0,\pm 1}(-1)^{2J'-M-\Omega'}[(2J'+1)(2J+1)]^{1/2} \\
& \times\begin{pmatrix} J' & 1 & J \\ -M & 0 & M \end{pmatrix}\begin{pmatrix} J' & 1 & J \\ -\Omega' & q & \Omega \end{pmatrix}\left[g_L\Lambda\delta_{\Sigma\Sigma'}+(g_S+g_r)(-1)^{S-\Sigma'}\right. \\
& \left.\times\begin{pmatrix} S & 1 & S \\ -\Sigma' & q & \Sigma \end{pmatrix}[S(S+1)(2S+1)]^{1/2}\right]-g_r\mu_B B_0M\delta_{JJ'}\delta_{\Sigma\Sigma'}\delta_{\Omega\Omega'} \quad (C7)
\end{aligned}$$

## REFERENCES

- Asensio Ramos, A., & Trujillo Bueno, J. 2003, in *Solar Polarization 3*, ed. J. Trujillo Bueno & J. Sánchez Almeida, ASP Conf. Ser. Vol 307, 195
- Asensio Ramos, A., & Trujillo Bueno, J. 2005, *ApJ*, in preparation

- Asensio Ramos, A., Trujillo Bueno, J., Bianda, M., Manso Sainz, R., & Uitenbroek, H. 2004a, *ApJ*, 611, L61
- Asensio Ramos, A., Trujillo Bueno, J., Carlsson, M., & Cernicharo, J. 2003, *ApJ*, 588, L61
- Asensio Ramos, A., Trujillo Bueno, J., & Collados, M. 2004b, *ApJ*, 603, L125
- . 2005, *ApJ*, 623, L57
- Bagnulo, S. 2003, in *Solar Polarization 3*, ed. J. Trujillo Bueno & J. Sánchez Almeida, ASP Conf. Ser. Vol 307, 505
- Ballik, E. A., & Ramsay, D. A. 1963, *ApJ*, 137, 61
- Berdyugina, S., Solanki, S. K., & Stenflo, J. O. 2003, in *Solar Polarization 3*, ed. J. Trujillo Bueno & J. Sánchez Almeida, ASP Conf. Ser. Vol 307, 181
- Berdyugina, S. V., & Solanki, S. K. 2001, *A&A*, 380, L5
- . 2002, *A&A*, 385, 701
- Brink, D. M., & Satchler, G. R. 1968, *Angular Momentum* (Oxford University Press)
- Brown, J. M., & Carrington, A. 2003, *Rotational Spectroscopy of Diatomic Molecules* (Cambridge: Cambridge University Press)
- Brown, J. M., Colbourn, E. A., Watson, J. K. G., & Wayne, F. D. 1979, *J. Mol. Spectrosc.*, 74, 294
- Brown, J. M., Kaise, M., Kerr, C. M. L., & Milton, D. J. 1978, *Molec. Phys.*, 36, 553
- Crawford, F. H. 1934, *Rev. Mod. Phys.*, 6, 90
- Edmonds, A. R. 1960, *Angular Momentum in Quantum Mechanics* (Princeton University Press)
- Gandorfer, A. 2000, *The Second Solar Spectrum, Vol. I: 4625 Å to 6995 Å* (Zurich: vdf)
- Gandorfer, A. 2003, in *Solar Polarization 3*, ed. J. Trujillo Bueno & J. Sánchez Almeida, ASP Conf. Ser. Vol 307, 399
- Goorvitch, D. 1990, *ApJS*, 74, 769
- Harvey, J. W. 1973, *Sol. Phys.*, 28, 43
- Harvey, J. W. 1985, in *Measurements of Solar Vector Magnetic Fields*, ed. M. J. Hagyard, NASA CP-2374, 109
- Herzberg, G. 1950, *Molecular Spectra and Molecular Structure. I. Spectra of Diatomic Molecules* (New York: Van Nostrand Company)



- Hill, E. L. 1929, *Phys. Rev.*, 34, 1507
- Huber, K. P., & Herzberg, G. 2003, in *Constants of Diatomic Molecules* (data prepared by J. W. Gallagher and R.D. Johnson, III), ed. P. J. Linstrom & W. G. Mallard, NIST Chemistry WebBook, NIST Standard Reference Database Number 69 (Gaithersburg MD: National Institute of Standards and Technology)
- Illing, R. M. E. 1981, *ApJ*, 248, 358
- Johnson, J. R., & Larson, H. P. 1983, *ApJ*, 270, 769
- Judd, B. R. 1975, *Angular Momentum Theory for Diatomic Molecules* (New York: Academic Press)
- Kronig, R. d. L. 1928, *Phys. Rev.*, 31, 195
- Landi Degl’Innocenti, E. 2003a, *Astronomische Nachrichten*, 324, 393
- Landi Degl’Innocenti, E. 2003b, in *Solar Polarization 3*, ed. J. Trujillo Bueno & J. Sánchez Almeida, ASP Conf. Ser. Vol 307, 164
- Landi Degl’Innocenti, E., & Landolfi, M. 2004, *Polarization in Spectral Lines* (Kluwer Academic Publishers)
- Langer, W. D., Velusamy, T., Kuiper, T. B. H., Levin, S., Olsen, E., & Migenes, V. 1995, *ApJ*, 453, 293
- Mathys, G. 2002, in *Astrophysical Spectropolarimetry*, ed. J. Trujillo Bueno, F. Moreno-Insertis, & F. Sánchez, *Proceedings of the XII Canary Islands Winter School of Astrophysics* (Cambridge, UK: Cambridge University Press), 101
- Press, W. H., Teukolsky, S. A., Vetterling, W. T., & Flannery, B. P. 1986, *Numerical Recipes* (Cambridge: Cambridge University Press)
- Rüedi, I., Solanki, S. K., Livingston, W., & Harvey, J. 1995, *A&AS*, 113, 91
- Schadee, A. 1978, *J. Quant. Spec. Radiat. Transf.*, 19, 517
- Shinnaga, H., & Yamamoto, S. 2000, *ApJ*, 544, 330
- Stenflo, J. O. 2002, in *Astrophysical Spectropolarimetry*, ed. J. Trujillo Bueno, F. Moreno-Insertis, & F. Sánchez, *Proceedings of the XII Canary Islands Winter School of Astrophysics* (Cambridge, UK: Cambridge University Press), 55
- Stenflo, J. O. 2003, in *Polarimetry in Astronomy*, ed. S. Fineschi, *Proceedings of the SPIE Vol. 4843* (SPIE), 76
- Stenflo, J. O., & Keller, C. U. 1996, *Nature*, 382, 588

—. 1997, *A&A*, 321, 927

Trujillo Bueno, J. 2003a, in *Solar Polarization 3*, ed. J. Trujillo Bueno & J. Sánchez Almeida, ASP Conf. Ser. Vol 307, 407

Trujillo Bueno, J. 2003b, in *Stellar Atmosphere Modeling*, ed. I. Hubeny, D. Mihalas, & K. Werner, ASP Conf. Ser. 288 (San Francisco: ASP), 551

Trujillo Bueno, J., Shchukina, N., & Asensio Ramos, A. 2004, *Nature*, 430, 326

Uitenbroek, H., Miller-Ricci, E., Asensio Ramos, A., & Trujillo Bueno, J. 2004, *ApJ*, 604, 960

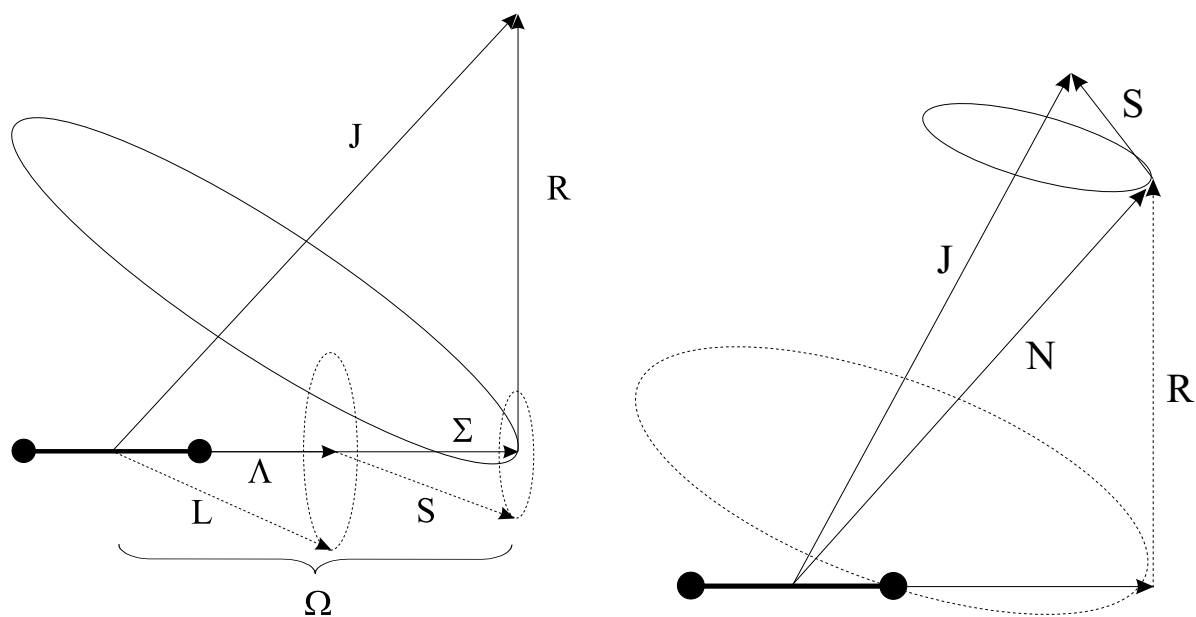


Fig. 11.— Vector diagram for Hund's case (a) (left panel) and Hund's case (b) (right panel). After Herzberg (1950).